

1 TGF β signalling is required to maintain pluripotency of human naïve pluripotent stem cells

2

3

4

5 Anna Osnato^{1,2}, Stephanie Brown^{1,2}, Christel Krueger³, Simon Andrews³, Amanda J. Collier⁴,
6 Shota Nakanoh^{1,2,5}, Mariana Quiroga Londoño^{1,2}, Brandon T. Wesley^{1,2}, Daniele Muraro^{1,2,6},
7 Sophie Brumm⁷, Kathy Niakan^{7,8}, Ludovic Vallier^{1,2,9}, Daniel Ortmann^{1,2,9}, Peter J. Rugg-
8 Gunn^{1,4,8,9}

9

10

11 ¹Wellcome–MRC Cambridge Stem Cell Institute, Jeffrey Cheah Biomedical Centre,
12 University of Cambridge, Cambridge, CB2 0AW, UK

13 ²Department of Surgery, University of Cambridge, Cambridge, CB2 0SZ, UK

14 ³Bioinformatics Group, The Babraham Institute, Cambridge, CB22 3AT, UK

15 ⁴Epigenetics Programme, The Babraham Institute, Cambridge, CB22 3AT, UK

16 ⁵Division of Embryology, National Institute for Basic Biology, Okazaki 444-8787, Japan

17 ⁶Wellcome Sanger Institute, Hinxton, Cambridge, CB10 1SA, UK

18 ⁷Human Embryo and Stem Cell Laboratory, The Francis Crick Institute, London, NW1 1AT,
19 UK

20 ⁸Centre for Trophoblast Research, University of Cambridge, Cambridge, CB2 3EG, UK

21 ⁹These authors jointly supervised this work

1 **Abstract**

2 The signalling pathways that maintain primed human pluripotent stem cells (hPSCs) have been
3 well characterised, revealing a critical role for TGF β /Activin/Nodal signalling. In contrast, the
4 signalling requirements of naïve human pluripotency have not been fully established. Here, we
5 demonstrate that TGF β signalling is required to maintain naïve hPSCs. The downstream
6 effector proteins – SMAD2/3 – bind common sites in naïve and primed hPSCs, including
7 shared pluripotency genes. In naïve hPSCs, SMAD2/3 additionally bind to active regulatory
8 regions near to naïve pluripotency genes. Inhibiting TGF β signalling in naïve hPSCs causes
9 the downregulation of SMAD2/3-target genes and pluripotency exit. Single-cell analyses
10 reveal that naïve and primed hPSCs follow different transcriptional trajectories after inhibition
11 of TGF β signalling. Primed hPSCs differentiate into neuroectoderm cells, whereas naïve
12 hPSCs transition into trophectoderm. These results establish that there is a continuum for TGF β
13 pathway function in human pluripotency spanning a developmental window from naïve to
14 primed states.

1 Introduction

2 Human pluripotent stem cells (hPSCs) are grown *in vitro* as two broadly different states termed
3 naïve and primed (Davidson et al., 2015; Weinberger et al., 2016). The two states diverge in
4 their embryonic identity with primed hPSCs recapitulating post-implantation epiblast, and
5 naïve hPSCs resembling pluripotent cells of pre-implantation embryos (Rossant and Tam,
6 2017; Weinberger et al., 2016). This difference has profound consequences on the cell's
7 properties, including the epigenetic state and differentiation capacity (Dong et al., 2019). Naïve
8 hPSCs have decreased DNA methylation levels, altered distribution of histone marks, and two
9 active X-chromosomes, and they have a higher propensity to differentiate into extraembryonic
10 tissues (Castel et al., 2020; Cinkornpumin et al., 2020; Dong et al., 2020; Guo et al., 2021; Io
11 et al., 2021; Linneberg-Agerholm et al., 2019; Pastor et al., 2016; Sahakyan et al., 2017;
12 Takashima et al., 2014; Theunissen et al., 2016; Vallot et al., 2017). On the other hand, primed
13 hPSCs represent the last stage before differentiation into the three definitive germ layers –
14 ectoderm, mesoderm and endoderm – from which the adult organs are derived (Weinberger et
15 al., 2016).

16 Importantly, these pluripotent states are established by using specific and distinct
17 culture conditions (Taei et al., 2020). Of particular interest, primed hPSCs rely on
18 TGF β /Activin/Nodal signalling to maintain their self-renewal and differentiation capacity
19 (James et al., 2005; Vallier et al., 2005). Inhibition of these pathways or knock down of their
20 effectors – SMAD2/3 – result in the rapid differentiation towards the neuroectoderm lineage
21 (Smith et al., 2008). Conversely, an increased activity of these signalling pathways is necessary
22 for endoderm differentiation (D'Amour et al., 2005; Touboul et al., 2010). The mechanisms
23 behind these apparent divergent functions remain to be fully uncovered, but the capacity of
24 SMAD2/3 to switch partners during differentiation is likely to play a key role (Brown et al.,
25 2011). Of note, Epiblast Stem Cells (EpiSCs) derived from post-implantation mouse embryos
26 also rely on TGF β /Activin/Nodal signalling (Brons et al., 2007). Furthermore, genetic studies
27 in the mouse have shown that Nodal signalling is necessary to block neuroectoderm
28 differentiation and to maintain the expression of pluripotency markers in the post-implantation
29 epiblast (Camus et al., 2006; Mesnard et al., 2006). Thus, the central role of
30 TGF β /Activin/Nodal in primed pluripotency seems to be evolutionary conserved and is
31 important for normal development.

32 In contrast, the function and evolutionary conservation of TGF β /Activin/Nodal
33 signalling in pre-implantation embryos is less well understood. TGF β /Activin/Nodal signalling
34 does not have an essential role in forming the pre-implantation epiblast in mouse (Brennan et

1 al., 2001; Varlet et al., 1997), whereas recent studies have suggested that the same pathway
2 may be necessary for epiblast development in human blastocysts (Blakeley et al., 2017). The
3 mechanistic basis for these observations are unclear. Moreover, it also remains to be
4 established whether TGF β signalling is required to maintain naïve hPSCs, which are the *in*
5 *vitro* counterparts of pre-implantation epiblast cells. In general, naïve pluripotency is believed
6 to be a steady state induced predominantly by blocking differentiation signals. However, the
7 culture conditions vary between laboratories, although interestingly, most media that support
8 naïve hPSCs contain exogenous TGF β /Activin or a source of TGF β provided by inactivated
9 fibroblasts or Matrigel-coated substrates (Bayerl et al., 2021; Chan et al., 2013; Gafni et al.,
10 2013; Guo et al., 2016; Takashima et al., 2014; Theunissen et al., 2014). Collectively, these
11 observations suggest there could be an uncharacterised role for TGF β /Activin/Nodal signalling
12 specifically in the human naïve pluripotent state.

13 Here we address this hypothesis by first establishing that TGF β /Activin/Nodal
14 signalling is active in naïve hPSCs. Using genome-wide analyses, we then show that SMAD2/3
15 is bound near to genes that characterise the naïve pluripotent state. Furthermore, loss of
16 function experiments demonstrate that this signalling pathway is necessary to maintain the
17 expression of key pluripotency genes, such as *NANOG*. We then perform single-cell RNA
18 sequencing analyses on naïve and primed hPSCs that are undergoing differentiation following
19 the inhibition of TGF β /Activin/Nodal signalling. In these conditions, primed hPSCs rapidly
20 decrease pluripotency markers and activate neuroectoderm genes, whereas naïve hPSCs induce
21 trophoctoderm markers. Importantly, these analyses also suggest that SMAD2/3 directly
22 maintains an important part of the transcriptional network characterising the naïve state. Taken
23 together, these results show that TGF β /Activin/Nodal signalling is necessary to maintain the
24 pluripotent state of naïve hPSCs through directly sustaining the expression of key pluripotency
25 genes. These new insights suggest that the function of TGF β /Activin/Nodal signalling in
26 human pluripotency extends to earlier stages of development than previously anticipated,
27 thereby underlying a key species divergence that could facilitate the identification and the
28 isolation of pluripotent states *in vitro*.

1 Results

2

3 TGF β signalling pathway is active in human naïve pluripotent cells

4 To assess whether the key effectors of the TGF β signalling pathway are expressed in naïve
5 hPSCs and to evaluate the cell heterogeneity in their expression (Figure 1a; Figure supplement
6 1a, b), we performed single cell transcriptomic analysis (scRNA-seq) in naïve and primed
7 hPSCs (Figure 1b, Figure supplement 1c). As expected, naïve and primed hPSCs clustered
8 separately based on their transcriptomes. All cells expressed pan-pluripotency genes, such as
9 *POU5F1* (also known as *OCT4*), *NANOG* and *SOX2*, however, naïve cells uniquely expressed
10 known naïve cell markers, such as *DPPA5* and *KLF4*, and primed cells expressed *CD24* and
11 *ZIC2* (Figure 1c, d; Figure supplement 1c). In addition, differential expression analysis
12 confirmed the specific expression of naïve hPSCs genes, such as *KLF4*, *DPPA3* and *TFCP2L1*,
13 and primed hPSCs factors including *DUSP6*, *ZIC2* and *TCF4* (Figure 1d). Importantly, we
14 found that most TGF β pathway effectors, such as Activin receptors (*ACVRs*) and *SMAD2-4*,
15 are expressed at similar levels in both pluripotent cell types (Figure 1e). Interestingly, several
16 components, including *NODAL* and *GDF3*, have higher expression levels in naïve compared
17 to primed hPSCs (Figure 1e).

18 We next examined RNA-seq datasets that covered different stages of human
19 pluripotency in stem cell lines and in embryos (Figure 1f). We first compared naïve and primed
20 hPSCs (Collier et al., 2017) and, consistent with our scRNA-seq data, we found that most
21 ligands, transduction proteins and receptors of the TGF β pathway are expressed at similar
22 levels in the two cell types (Figure 1f). Higher expression of the TGF β ligands *NODAL* and
23 *GDF3* and the co-receptor *TDGF1* was again detected in naïve hPSCs. Interestingly, the
24 expression of pathway inhibitors differed, whereby *LEFTY1* and *LEFTY2* were higher in naïve
25 hPSCs, whereas *CER1* and *FST* were higher in primed hPSCs. We then looked at gene
26 expression changes that occur during the process of capacitation, because the transition from
27 naïve to primed hPSCs recapitulates pre- to post-implantation epiblast cell development
28 (Rostovskaya et al., 2019). We found that most of the effectors of the TGF β pathway are
29 expressed throughout the entire developmental series, and also confirmed that *NODAL* and
30 *GDF3* are expressed at higher levels in the early stages (Figure 1f).

31 To examine transcriptional events directly in human embryos, we next looked at
32 scRNA-seq data in human pre-implantation embryos from day 3 to day 7 (Petropoulos et al.,
33 2016). Low level expression of most TGF β pathway effectors was detected in the early inner
34 cell mass (ICM), and their expression increased substantially in the pre-implantation epiblast

1 (EPI). In particular, *NODAL* and *GDF3* are highly expressed in EPI at this stage, similar to the
2 transcriptional patterns in naïve hPSCs (Figure 1f). However, in contrast to EPI, most pathway
3 components are undetectable in trophectoderm (TE and early TE), and are expressed at low
4 levels in primitive endoderm (PE) (Figure 1f). These observations were extended by examining
5 the expression of TGF β pathway genes in a blastocyst-culture system that recapitulates EPI
6 development from pre-implantation to early gastrulation (Xiang et al., 2020). Here, in EPI cells
7 at 6 days post-fertilisation, *NODAL*, *GDF3* and the NODAL co-receptor *TDGFI* are highly
8 expressed, in line with the EPI stage from the Petropoulos et al. dataset, and the high expression
9 of these genes is sustained in all EPI cells over the following eight days of development (Figure
10 1f). Taken together, these results show that most ligands, transduction proteins and receptors
11 of the TGF β pathway are expressed at similar levels in naïve and primed hPSCs, and that this
12 expression pattern across pluripotent states is also observed in human embryos cultured *in*
13 *vitro*.

14 To further confirm these observations at the protein level, we examined cell-surface
15 proteomic (Wojdyla et al., 2020) and whole-cell proteomic (Di Stefano et al., 2018) data in
16 naïve and primed hPSCs. This revealed that most Activin/TGF β receptors and downstream
17 effectors of the pathways are expressed at very similar levels in the two cell types (Figure 1g,
18 Figure supplement 1d). Finally, to directly assess TGF β pathway activation, we performed
19 western blot analysis and found that phospho-SMAD2 (pSMAD2), the activated form of
20 SMAD2, is detectable in multiple embryo-derived and reprogrammed naïve hPSCs lines, and
21 at comparable levels to primed cells (Figure 1h; Figure supplement 1e, f). The phosphorylation
22 signal was rapidly diminished following the treatment of the cells with SB-431542 (SB), a
23 potent and selective inhibitor that blocks TGF β /Activin receptors ALK5, ALK4, and ALK7
24 (Inman et al., 2002) (Figure 1h; Figure supplement 1e, f). Taken together, these results establish
25 that the TGF β signalling pathway is active in naïve hPSCs. Because primed hPSCs rely on this
26 pathway to maintain pluripotency, our findings raise the possibility that naïve hPSCs might
27 also require TGF β signalling to sustain their undifferentiated state.

28

29 **SMAD2/3 binding is enriched at active enhancers in human naïve cells**

30 Having established that the TGF β signalling pathway is active in naïve hPSCs, we next profiled
31 the genome-wide occupancy of the main downstream effectors – SMAD2/3 – using chromatin
32 immunoprecipitation combined with genome-wide sequencing (ChIP-seq) in naïve and primed
33 hPSCs. This analysis revealed that SMAD2/3 binding is enriched in naïve cells to a similar
34 degree as in primed cells, as shown by independent peak calling in the two cell types (Figure

1 2a; Figure supplement 2a). Here, we observed regions bound by SMAD2/3 in both cell types,
2 and also a substantial number of loci that appear to have cell type-specific binding. Importantly,
3 canonical target genes, such as *LEFTY1/2*, *NODAL*, *NANOG* and *SMAD7*, were bound by
4 SMAD2/3 in both cell types (Figure 2b; Figure supplement 2b), suggesting that TGF β is active
5 and it signals through the canonical cascade in both naïve and primed hPSCs.

6 In addition to the shared targets, differential binding analyses revealed over 2,000
7 SMAD2/3-bound sites that differed between the two cell types (Figure 2c, d; Figure
8 supplement 2c, d). Excitingly, further examination of these differential sites revealed that in
9 naïve hPSCs SMAD2/3 uniquely bound near to naïve-specific pluripotency genes including
10 *DNMT3L*, *TFAP2C*, *CBFA2T2*, *KLF4* and *CDK19* (Figure 2e; Figure supplement 2d, e).
11 Interestingly, these sites often overlapped with accessible chromatin regions and H3K27ac
12 marks, which are signatures that are associated with active enhancers (Heintzman et al., 2009)
13 (Figure 2e; Figure supplement 2e). In contrast, primed-specific SMAD2/3 sites were located
14 near to genes that regulate mesendoderm differentiation, such as *TBXT*, *EOMES* and *GATA4*,
15 or primed-state pluripotency, such as *OTX2* (Figure 2e, Figure supplement 2e). These sites
16 correspond mostly to accessible chromatin and to regions marked by H3K4me3 and
17 H3K27me3 signals, which typically mark the promoters of developmental genes (Azuara et
18 al., 2006; Bernstein et al., 2006; Heintzman et al., 2009) (Figure 2e; Figure supplement 2e).
19 These findings are supported by global analysis using ChromHMM-based chromatin state
20 annotations (Chovanec et al., 2021), where we found that most SMAD2/3 peaks are indeed
21 within active chromatin regions, consisting mainly of gene promoters and enhancers (Figure
22 2f). Interestingly, naïve-specific SMAD2/3 peaks are slightly more enriched at active
23 enhancers compared to primed-specific peaks (30.6% vs 21.4%), and primed-specific
24 SMAD2/3 peaks are instead more enriched at promoters (46% vs 26.5%) (Figure 2f; Figure
25 supplement 2f).

26 There are widespread differences in enhancer activity between naïve and primed hPSCs
27 (Barakat et al., 2018; Battle et al., 2019; Chovanec et al., 2021) and so to determine how
28 changes in SMAD2/3 occupancy tracks with enhancer status we compared chromatin marks at
29 naïve-specific SMAD2/3 sites between the two cell types. The vast majority of sites that lose
30 SMAD2/3 occupancy in primed hPSCs also show a strong reduction in chromatin accessibility
31 and H3K27ac/H3K4me1 signals, which suggests that SMAD2/3-bound enhancers are
32 decommissioned in primed hPSCs (Figure 2g). Chromatin marks that denote promoters and
33 heterochromatin regions are generally low at naïve-specific SMAD2/3 sites and are largely

1 unchanged in primed hPSCs, further reinforcing the connection between SMAD2/3 occupancy
2 and active enhancers in naïve hPSCs (Figure 2h).

3 To obtain a more complete view of the pluripotency transcriptional network, we also
4 overlapped SMAD2/3 peaks in naïve cells with OCT4, SOX2 and NANOG (OSN) binding
5 (Chovanec et al., 2021). We found that OSN signals were strongly reduced at naïve-specific
6 SMAD2/3 sites in primed hPSCs, confirming the integration of SMAD2/3 within the naïve
7 transcription factor network (Figure 2i). Importantly, regions bound by SMAD2/3 and OSN
8 overlapped with state-specific enhancers that are marked by open chromatin and H3K27ac, as
9 shown for the *KLF4* and *DNMT3L* loci in naïve hPSCs, and for *OTX2* and *TBXT* in primed
10 hPSCs (Figure 2e). Finally, to further characterise the differentially bound loci, we performed
11 differential motif enrichment to investigate whether different binding partners might regulate
12 SMAD2/3 binding in naïve and primed cells. Interestingly, motifs that are relatively enriched
13 at SMAD2/3 sites in naïve compared to primed cells included NF2L1 (also known as NRF1),
14 TFAP2A/C, KLF4 and FOXH1 (Figure 2j).

15 Altogether, these data suggest that SMAD2/3, the main effector of TGF β pathway, is
16 integrated in the naïve pluripotency network by targeting OSN-bound active enhancers that are
17 in close proximity to key regulators of naïve pluripotency.

18

19 **Inhibiting TGF β signalling induces loss of pluripotency in human naïve cells**

20 After establishing that the TGF β signalling pathway could maintain directly the transcriptional
21 network characterising human pluripotency, spanning from naïve to primed states, we next
22 examined whether the pathway is functionally required to sustain naïve hPSCs in an
23 undifferentiated state. We first measured the transcriptional changes that occurred in response
24 to SB-mediated loss of pSMAD2 and inhibition of the TGF β pathway (Figure 3a; Figure
25 Supplement 3a, b). After only two hours of SB treatment (t2iLGö medium supplemented with
26 SB), naïve hPSCs showed a significant reduction in the expression of the pluripotency gene
27 *NANOG*, which is a short time frame that is consistent with *NANOG* being a direct target of
28 SMAD2/3 signalling (Vallier et al., 2009; Xu et al., 2008) (Figure 3a, Figure supplement 3a).
29 Other canonical downstream target genes, such as *LEFTY1/2* and *SMAD7*, were also strongly
30 downregulated and their expression was completely abolished after 24 hours in the case of
31 *LEFTY1/2*. Excitingly, naïve pluripotency marker genes that are bound by SMAD2/3 including
32 *DPPA3*, *DPPA5*, *KLF4* and *DNMT3L* were also downregulated following SB treatment,
33 indicating that the naïve state is disrupted in these conditions (Figure 3a, Figure supplement
34 3a). These results were independently validated by depleting SMAD2/3 expression using the

1 OPTiKD system (Bertero et al., 2016). Here, we generated stable naïve hPSCs with tetracycline
2 (TET) inducible co-expression of shRNAs that target *SMAD2* and *SMAD3* transcripts (Figure
3 3b). Treating these cells with TET induced the rapid loss of *SMAD2/3* mRNA (Figure 3c), and
4 a concomitant and significant downregulation in the expression of *SMAD2/3* target genes, such
5 as *LEFTY2*, *NODAL* and *NANOG* (Figure 3c). We also detected a significant decrease in
6 *POU5F1* expression following *SMAD2/3* knockdown and after SB treatment, suggesting that
7 naïve hPSCs are destabilised and are exiting the pluripotent state (Figure 3a, c).

8 Interestingly, adding SB to naïve culture media also induced a change in cell
9 morphology whereby naïve hPSCs lost their typical dome-shaped morphology after 3 to 5 days,
10 and this was accompanied by the appearance of flat colonies that gradually took over the culture
11 (Figure 3d, Figure supplement 3c). This striking phenotypic change was confirmed in a second
12 naïve hPSCs line (Figure supplement 3d). Intriguingly, the morphology of these flat colonies
13 resemble human trophoblast cells (Okoe et al., 2018). To further investigate this, we grew naïve
14 hPSCs for 14 days in the presence of SB and then examined the expression of trophoblast
15 marker genes (Figure 3e). We found there was a strong upregulation in the expression of the
16 trophoblast marker *HAND1* and also of *TP63*, *MMP2* and *SDCI* that mark cytotrophoblast
17 (CTB), extravillous trophoblast (ETV) and syncytiotrophoblast (STB) cell types, respectively
18 (Figure 3e). These results were further supported by the clear reduction in *NANOG* protein
19 expression following 3 to 5 days of treating naïve hPSCs with SB, in correspondence with the
20 exit from naïve pluripotency and the appearance of the trophoblast-like colonies (Figure 3f).
21 *NANOG* downregulation together with the appearance of trophoblast-like colonies was also
22 observed in a second naïve cell line upon SB treatment (Figure supplement 3e). Importantly,
23 the flat cell colonies also expressed typical trophoblast-associated proteins – *GATA3* and
24 *HAND1* (Figure 3g, Figure supplement 3f, g).

25 To further characterise these cells and to investigate their ability to differentiate into
26 trophoblast derivatives, we cultured naïve hPSCs in the presence of SB for 5 days and then
27 transferred the cells into trophoblast stem cell (TSC) media (Dong et al., 2020; Okoe et al.,
28 2018). Although the cell population initially appeared heterogeneous, following exposure to
29 TSC conditions the cells rapidly and uniformly acquired a homogeneous TSC-like
30 morphology. The cells expressed TSC markers, such as *GATA3* and *CK19* (Figure 3h) and
31 *CK7*, *ITGA6* and *TP63* (Figure 3i), and could be passaged and maintained in these conditions
32 with stable growth and morphology. Naïve-derived TSCs were then induced to differentiate by
33 switching the cells to STB and EVT media (Dong et al., 2020). This led to the downregulation

1 of TSC genes and the upregulation of STB and EVT markers, such as SDC1 and HLA-G,
2 respectively (Figure 3h, i).

3 Taken together, these results show that blocking TGF β signalling in naïve hPSCs
4 rapidly destabilises the pluripotency network and allows the cells to undergo differentiation
5 towards trophoblast-like cells, including those that can give rise to multipotent, proliferative
6 TSCs.

7 8 **Single-cell transcriptional analysis reveals a trophoblast-like population arising in** 9 **response to TGF β inhibition in human naïve cells**

10 We next sought to investigate the processes in which TGF β pathway inhibition drives naïve
11 hPSCs out of their pluripotent state and towards a trophoblast phenotype. Following SB
12 treatment, we observed that the early-stage cultures contained a heterogeneous mixture of cell
13 morphologies that included naïve-like colonies and the flat, TSC-like colonies described above
14 (Figure 3d, Figure supplement 3c, d). The proportion of NANOG-positive cells declined
15 following SB treatment, with variable expression within individual colonies (Figure 3f). We
16 also observed heterogeneous colonies that contained cells expressing the pluripotency marker
17 OCT4 and TSC-like markers HAND1/GATA3 (Figure 3g). Because the population
18 heterogeneity could mask important changes in cell phenotype, we used scRNA-seq to examine
19 the effect of TGF β inhibition over seven days of SB treatment in naïve hPSCs (Figure 4a). In
20 addition, to better characterise the divergent developmental potential between different human
21 pluripotent states, we compared this response to the response when primed hPSCs were treated
22 with SB. Our aim was to investigate the trajectory of naïve hPSCs moving into a putative TSC-
23 like population, in contrast with the neuroectodermal differentiation that is induced in primed
24 hPSCs when TGF β is inhibited (Vallier et al., 2009).

25 In both cell types, there was a clear transcriptional trajectory moving from day 0 to day
26 7 of SB treatment (Figure 4b, Figure supplement 4a). Importantly, there was little overlap in
27 their trajectories (Figure 4c), confirming that the inhibition of TGF β signalling in these two
28 different developmental stages results in divergent differentiation processes. Louvain
29 clustering of the combined datasets also showed separated clusters in the naïve and primed
30 time course samples (Figure supplement 4b). Specifically, TGF β inhibition in naïve hPSCs
31 induced the expression of TSC-like markers, such as *HAND1*, *GATA2* and *GATA3*, whereas
32 inhibition in primed hPSCs induced neuroectoderm markers, such as *SOX10*, *PAX6* and *LEF1*
33 (Figure 4d, Figure supplement 4c). Interestingly, Louvain clustering of the naïve cell dataset
34 initially follows the day 0 (Cluster A) and day 1 (Cluster B) timepoints and then resolves the

1 mixed population at days 3, 5 and 7 into three separate clusters (C, D and E) (Figure 4e, Figure
2 supplement 4d). This analysis suggests that the mixed population is formed from an early
3 differentiating population (cluster C), a transition population (cluster D), and a later-stage
4 differentiated population (cluster E), thereby confirming a stepwise process marked by
5 different intermediate stages.

6 Examining individual genes revealed the dynamics of the differentiation trajectory.
7 Pan-pluripotency and naïve-specific genes showed a gradient in their expression patterns,
8 starting from high expression in cluster A, diminishing levels in clusters B and C, then largely
9 absent in clusters D and E (Figure 4f, g). In contrast, trophoblast genes become activated in
10 clusters C, D and E, with *CDX2*, *HAND1* and *GATA3* marking early, transition and late-stage
11 differentiating populations, respectively (Figure 4f, g). *NODAL* and *LEFTY1* are expressed
12 predominantly in cluster A and were rapidly downregulated already in cluster B (Figure 4f, g),
13 and other TGF β pathway genes, such as *GDF3* and *TDGFI*, are fully downregulated when
14 cells start transitioning towards cluster D. These results confirm the effective pathway
15 inhibition and also that blocking TGF β signalling allows trophectoderm differentiation.

16 To better characterise the Louvain clusters, we examined the top 25 genes that are
17 differentially expressed in each cluster compared to all other clusters (Figure 4g, Figure
18 supplement 4e, f). Differentially expressed genes that are associated with cluster A, which
19 corresponds largely to cells at day 0, include *NANOG* and *SUSD2* (Bredenkamp et al., 2019a;
20 Wojdyla et al., 2020) in addition to the TGF β ligand *GDF3* and receptor *TDGFI*. Interestingly,
21 the SMAD2/3-cofactor *FOXH1* was also identified in this category and this is consistent with
22 our prior motif analysis of the SMAD2/3 ChIP-seq data that identified FOXH1 as a putative
23 interactor of SMAD2/3 specifically in naïve cells (Figure 2j). Genes that are differentially
24 expressed in cluster B are enriched for metallothioneins, such as MT1/2s, which affect cell
25 respiration, in addition to mitochondrial genes – *SLIRP* and *MTNDL4* – and the glucose
26 pyrophosphorylase *UGP2*, suggesting that an initial response to TGF β inhibition could involve
27 a metabolic switch (Mathieu and Ruohola-Baker, 2017). Cells in cluster C still express
28 pluripotency markers, such as *POU5F1* and *DPPA5*, and have upregulated the non-coding
29 RNAs *MEG3* and *MEG8*. Cluster D clearly marks a transition population towards TSC-like
30 cells, with the expression of *CDX1* and *CDX2*, keratins (*KRT8*, *KRT18*), and *MARCKS*, *FABP5*
31 and *EZR* (Cambuli et al., 2014; Ralston et al., 2010). Cluster E includes keratins (*KRT8*,
32 *KRT18*, *KRT19*), several main regulators of trophoblast development, such as *GATA2* and
33 *GATA3* (Ralston et al., 2010), and human specific regulators, such as *VGLLI* (Soncin et al.,
34 2018). Lastly, because recent studies have highlighted a transcriptional overlap between

1 trophoblast and amnion cells (Guo et al., 2021; Io et al., 2021; Zhao et al., 2021), we examined
2 whether genes reported to be expressed by amnion cells were upregulated in our dataset. We
3 found that most of the amnion-associated genes examined were not detectable in any of the
4 clusters (Figure supplement 4g). Some markers, such as *CTSV* and *TPMI*, are expressed in
5 both amnion and trophoblast, and as expected were upregulated in cluster E (Figure supplement
6 4g). Although it is currently challenging to separate the transcriptional profiles of trophoblast
7 and amnion cells, this analysis suggests that TGF β inhibition of naïve hPSCs in these
8 conditions does not promote the induction of reported amnion cell markers. Taken together,
9 these results confirm that TGF β inhibition downregulates a pluripotency program and enables
10 trophoctoderm differentiation from naïve hPSCs.

11 To dissect the impact of TGF β pathway inhibition on the transcriptional changes, we
12 overlapped cluster A and E gene expression profiles with SMAD2/3 ChIP-seq peaks. We found
13 that a small subset of differentially expressed genes have a nearby SMAD2/3 peak (Figure 4h).
14 Of note, many of the strongest peaks are close to differentially expressed genes, and this was
15 especially clear for genes that are downregulated upon SB treatment (Figure 4i). Interestingly,
16 among the downregulated genes, we found that SMAD2/3 bind within 12kb of the
17 transcriptional start sites of TGF β downstream effectors (*NODAL*, *LEFTY1/2*, *PMEPA1*), key
18 genes associated with naïve pluripotency (*DNMT3L*, *DPPA4*, *AIRE*, *IDI1*), genes reported to
19 inhibit trophoblast differentiation (*NLRP7*, *TET1*) (Alici-Garipcan et al., 2020; Dawlaty et al.,
20 2011; Koh et al., 2011; Mahadevan et al., 2014), and also near to distal enhancers for other
21 factors, such as *KLF4* and *DEPTOR* (Figure 4h). Although less prevalent, we also found
22 SMAD2/3 binding sites close to some genes that are transcriptionally upregulated between
23 cluster A and E, including *EFNB2* and *FOS*, and to enhancers close to *PGF* and *MFAP5*. To
24 further assess the significance of this association, we tested how often differentially expressed
25 genes between clusters A and E are the closest gene to a SMAD2/3 peak. Strikingly, 21% of
26 downregulated genes are the closest gene to a SMAD2/3 binding site, which is significantly
27 higher than the 7% of genes in a randomly-selected group of size-matched control genes
28 ($p < 2.2 \times 10^{-16}$, Figure 4j). These results suggest that the downregulation of pluripotency-
29 associated genes following TGF β inhibition is functionally linked to the loss of SMAD2/3
30 binding.

31 Taken together, scRNA-seq in primed and naïve cells shows that both developmental
32 stages rely on TGF β signalling to maintain their undifferentiated state but, upon pathway
33 inhibition, each cell type diverges towards different trajectories. Primed cells differentiate into
34 neuroectoderm cells whereas, in contrast, naïve cells exit pluripotency and acquire a TSC-like

1 fate expressing trophoblast markers and this is triggered by the deregulation of target genes
2 that are downstream of SMAD2/3.

3

4 **TGF β inhibition in naïve hPSCs recapitulates the transcriptome of early trophoblast** 5 **specification in human embryos**

6 Having established that naïve hPSCs respond to TGF β inhibition by shutting down the naïve
7 pluripotency network, thereby allowing the onset of trophoblast differentiation, we next
8 investigated whether this differentiation process follows a developmental trajectory. To do this,
9 we applied diffusion pseudotime to our 10X scRNA-seq data (Figure supplement 5a) and
10 examined the pseudotime trajectory across the Louvain clusters (Figure 5a). Consistent with
11 the prior UMAP analysis, we found that the time points (days) and the clusters progressively
12 populate the trajectory following a similar pattern from cluster A, through B and C, towards a
13 transition population in cluster D, and lastly the more differentiated counterpart in cluster E
14 (Figure 5a). Overlaying the diffusion pseudotime maps with the expression of known markers
15 reveals the initial downregulation of pluripotency genes, such as *NANOG*, was followed by a
16 sequential upregulation of trophoblast markers, such as *CDX2*, *HAND1* and *GATA3* (Figure
17 5b, Figure supplement 5b). Interestingly, the transitional cell population in cluster D contains
18 a substantial proportion of cells (~15-25%) that co-express low levels of the pluripotency gene
19 *POU5F1* and trophoblast markers, such as *CDX2* and *HAND1* (Figure 5c). We confirmed this
20 co-expression at the protein level using immunofluorescent microscopy (Figure supplement
21 5c). These results indicate that trophoblast cells arise in the population through the transition
22 of pluripotent cells to a trophoblast fate.

23 To further investigate the transition from naïve pluripotency to trophoblast
24 specification, we compared our scRNA-seq data to human embryo transcriptional datasets
25 (Xiang et al., 2020). Correlation analysis showed that cells in clusters A, B and C are
26 transcriptionally closest to epiblast cells, in keeping with their undifferentiated status (Figure
27 supplement 5d). The transitional population classified as cluster D has the highest correlation
28 with ICM and TE (Figure supplement 5d). Cells in cluster E have the highest correlation with
29 trophoblast derivatives from the pre- and early-postimplantation embryo (Figure supplement
30 5d).

31 We next focussed our analysis on the main pluripotent cell population (cluster A), the
32 transitioning cells (cluster D) and the differentiated cells (cluster E). We compared these
33 clusters with the embryo cell types that showed the highest transcriptional correlations to them
34 (Figure 5d and Figure supplement 5d). Visualising single cell transcriptomes for each cell type

1 on a PCA plot revealed there was a good overlap between our stem cell differentiation series
2 and the embryo lineages (Figure 5e), further supporting a transition from EPI to the trophoblast
3 lineage. We then used the Wilcoxon Rank Sum test to identify marker genes for each embryo
4 lineage and examined the expression pattern of those genes in cells across clusters A, D and E.
5 Interestingly, the two datasets have remarkably similar expression patterns, whereby the
6 progression from clusters A to D to E closely resembles the transcriptional changes from EPI
7 to trophoblast (Figure 5f). Among the top 20 genes per cluster (Figure supplement 5e), we
8 found genes, such as *NANOG* and *DPPA5* for cluster A / EPI, and trophoblast markers, such
9 as *VGLL1* and *PGF* for cluster E / trophoblast, and confirmed their expression at the single cell
10 level over the differentiation pseudotime (Figure 5g). Taken together, these results reveal that
11 TGF β inhibition of naïve hPSCs causes the cells to initiate a differentiation programme from
12 pluripotency to TE-like cells and trophoblast derivatives, activating transcriptional identities
13 similar to the embryo counterpart

14
15

16 **Discussion**

17 Here we show that TGF β /Activin/Nodal signalling is active in naïve hPSCs and that this
18 pathway is required to maintain the cells in an undifferentiated state. These findings, therefore,
19 establish that there is a continuum for TGF β signalling function in pluripotency spanning a
20 developmental window from naïve to primed states (Figure 5h).

21 Until now, the role of TGF β signalling in naïve hPSCs has been unclear. Activators of
22 this pathway are often included in naïve hPSCs culture formulations (Bayerl et al., 2021; Chan
23 et al., 2013; Theunissen et al., 2014), suggesting that this pathway could be necessary to
24 maintain pluripotency. Accordingly, we show here that naïve hPSCs transcribe high levels of
25 endogenous TGF β ligands and receptors, and the pathway is activated in standard naïve cell
26 growth conditions as demonstrated by the phosphorylation status of SMAD2/3. These findings
27 help to interpret previous observations from several studies. For example, when testing
28 different culture formulations, the removal of Activin from 5iLA conditions led to an increase
29 in the spontaneous differentiation of naïve hPSCs, and also to the reduced expression of naïve
30 genes, including *NANOG* and *KLF4* (Theunissen et al., 2014). Furthermore, supplementing
31 HENSM media with Activin caused naïve hPSCs to express higher levels of *KLF17*, *DNMT3L*
32 and *DPPA3* (genes that are confirmed as SMAD2/3 targets in our study) and elevated *POU5F1*
33 distal enhancer activity, compared to the same conditions without Activin (Bayerl et al., 2021).
34 In addition to the effect on established naïve cell lines, Activin also enhanced the kinetics of

1 primed to naïve hPSCs reprogramming (Theunissen et al., 2014). At the time, the authors
2 speculated that Activin prolongs primed hPSCs in a state that is amenable to naïve
3 reprogramming. Based on the results from our study, we propose that TGF β signalling is
4 required to maintain pluripotency in cells throughout primed to naïve cell reprogramming and
5 additionally enforce the expression of genes that promote naïve hPSCs. Thus,
6 TGF β /Activin/Nodal signalling helps to stabilise naïve pluripotency and the addition of Activin
7 to naïve induction and maintenance conditions is predicted to be beneficial.

8 At the molecular level, our analysis showed that SMAD2/3, the DNA-binding effectors
9 downstream of TGF β /Activin/Nodal signalling, occupied genomic sites that were common to
10 both naïve and primed hPSCs, in addition to a large set of cell type-specific sites. Shared target
11 genes included core pluripotency factors, such as *NANOG*, in addition to factors that are
12 canonical targets, such as *LEFTY1/2* and *SMAD7*. Disrupting TGF β signalling in naïve and
13 primed hPSCs caused the rapid downregulation of these common target genes, indicating the
14 presence of shared gene regulatory networks between the two pluripotent states. We
15 additionally identified a large set of genes that were targeted by SMAD2/3 in naïve hPSCs but
16 not in primed hPSCs. This set of genes included *KLF4*, *TFAP2C* and *DNMT3L*, which are
17 important regulators of naïve pluripotency (Bayerl et al., 2021; Pastor et al., 2018), and we
18 demonstrated that their expression levels were also sensitive to TGF β pathway inhibition.
19 These findings indicate that TGF β /Activin/Nodal signalling functions in naïve hPSCs to
20 reinforce the expression of key genes that promote naïve pluripotency, rather than to repress
21 differentiation-promoting factors. Previous studies suggest that TGF β /Activin/Nodal
22 signalling may regulate *NANOG* expression in human embryos (Blakeley et al., 2017). It will
23 be important to determine in the future whether the signalling requirements we uncover in
24 naïve hPSCs could also be operating in pluripotent cells of human embryos. If so, then existing
25 naïve hPSCs may serve as a useful cell model in which to investigate the mechanisms of
26 signalling pathways that are relevant for early human development, alternatively, if this shows
27 distinctions it may point to ways in which current *in vitro* conditions may need to be further
28 refined to more closely recapitulate the pre-implantation embryonic epiblast in the embryo.
29 Importantly, genetic studies in the mouse have established a key function for Nodal-SMAD2/3
30 signalling in maintaining the pluripotent state of post-implantation epiblast and in the formation
31 of the primitive streak during gastrulation (Brennan et al., 2001; Varlet et al., 1997).
32 Concerning pre-implantation stages, TGF β /Activin/Nodal signalling appears to play a role in
33 the regionalisation of the extraembryonic endoderm. However, a function in the early epiblast

1 remains elusive, thereby suggesting the existence of species divergence regarding
2 TGF β /Activin/Nodal signalling function during early development.

3 Our experiments also uncovered a widespread relocalisation in the genomic sites that
4 are occupied by SMAD2/3. By integrating our datasets with chromatin and transcription factor
5 profiles, we found that SMAD2/3 binding was enriched at active enhancers in naïve cells, yet
6 predominantly at promoters in primed cells. This redistribution mirrors changes in OCT4,
7 SOX2 and NANOG occupancy, whereby sites bound by SMAD2/3 only in naïve hPSCs are
8 also preferentially occupied by OSN in naïve compared to primed cells. These findings predict
9 that SMAD2/3 and OSN integrate signalling and transcription factor inputs in naïve
10 pluripotency, similar to the functional interaction between SMAD2/3 and NANOG in primed
11 hPSCs (Brown et al., 2011; Xu et al., 2008). Together, these results establish that TGF β
12 signalling is a core feature that is closely integrated within the transcriptional network of naïve
13 hPSCs.

14 Finally, our single-cell analysis revealed that naïve and primed hPSCs depart along
15 different trajectories following TGF β inhibition. Primed hPSCs differentiated rapidly into
16 neuroectoderm following TGF β inhibition, which is consistent with previous studies (Smith et
17 al., 2008). In contrast, naïve hPSCs upregulated trophoblast-associated genes after several days
18 of TGF β inhibition. The divergent routes taken by naïve and primed hPSCs could be due to
19 their different developmental states and differentiation potential. In keeping with their
20 preimplantation epiblast identity, naïve hPSCs can differentiate efficiently into trophoblast and
21 hypoblast, and are required to transition through a process of capacitation to acquire the
22 competency to respond directly to signals that promote postimplantation germ layer induction.
23 In contrast, primed hPSCs are more similar to early postimplantation epiblast, and therefore do
24 not efficiently make trophoblast and hypoblast. Additionally, the presence of different factors
25 and inhibitors in the naïve and primed hPSC culture media could also affect their responses to
26 TGF β inhibition. Importantly, not all of the cells in the inhibitor-treated naïve cultures
27 differentiated uniformly over the first few days. Thus, we speculate that the presence of small
28 molecules inhibiting MEK, GSK3 β , and PKC with the addition of LIF can attenuate the effect
29 of TGF β inhibition (Guo et al., 2021). Notably, a TGF β inhibitor is a common component of
30 human TSC medium (Okae et al., 2018), which suggests that TGF β signalling may act to limit
31 trophoblast self-renewal or proliferation. TGF β inhibitors are also a component in the
32 conditions that can convert naïve hPSCs to TSCs (Castel et al., 2020; Cinkornpumin et al.,
33 2020; Dong et al., 2020; Liu et al., 2020). Here, the inhibitor might be functioning in two ways:
34 to induce the exit from naïve pluripotency, and to promote trophoblast cell growth.

1 Unexpectedly, our single cell analysis revealed that following TGF β inhibition, naïve cells
2 acquire a transcriptional identity closest to ICM and early TE, marked, for example, by
3 transient *CDX2* expression, and then the cells undergo further differentiation into trophoblast
4 cell types. *CDX1* and *CDX2* are expressed transiently in primate trophoblast development
5 including the pre-implantation TE in human blastocysts (Niakan and Eggan, 2013), but are not
6 expressed in embryo-derived TSCs or naïve hPSC-derived TSCs, which are more similar to
7 post-implantation trophoblast (Castel et al., 2020; Dong et al., 2020; Okae et al., 2018). By
8 capturing pre-implantation TE-like cells, our scRNA-seq data could, therefore, shed light on
9 the transcriptional changes that occur during the early stages of human trophoblast
10 specification.

11 To conclude, our results establish a central role for TGF β /Activin/Nodal signalling in
12 protecting human pluripotent stem cells against differentiation. This knowledge will be useful
13 to establish culture conditions allowing the derivation and production *in vitro* of different cell
14 types constituting the human embryo. In addition, modulation of TGF β could play a key role
15 in the early human embryo and could be useful for improving culture conditions used to grow
16 human embryos *in vitro*.

1 **Materials and Methods**

2

3 **Cell culture**

4 Transgene-reset WA09/H9 NK2, embryo-derived HNES1 and chemically-reset cR-H9 naïve
5 hPSCs (Guo et al., 2017, 2016; Takashima et al., 2014) were kindly provided by Dr. Austin
6 Smith with permission from WiCell and the UK Stem Cell Bank Steering Committee. Cells
7 were maintained in t2iLGö (Takashima et al., 2014) or in PGXL (Bredenkamp et al., 2019b;
8 Rostovskaya et al., 2019) in hypoxia (5% O₂) at 37°C. The N2B27 base medium contained a
9 1:1 mixture of DMEM/F12 and Neurobasal, 0.5X N-2 supplement, 0.5X B-27 supplement,
10 2mM L-Glutamine, 0.1mM β-mercaptoethanol (all from ThermoFisher Scientific), 0.5X
11 Penicillin/Streptomycin. For t2iLGö, the base medium was supplemented with 1μM
12 PD0325901, 1μM CHIR99021, 20ng/ml human LIF (all from WT-MRC Cambridge Stem Cell
13 Institute) and 2μM Gö6983 (Tocris). For PXGL, N2B27 medium was supplemented with 1μM
14 PD0325901, 2μM XAV939, 2μM Gö6983 and 10 ng/ml human LIF. Naïve hPSCs were
15 maintained on a layer of irradiated mouse fibroblasts that were seeded at a density of two
16 million cells per 6-well plate. All experiments have been performed on naïve hPSCs that were
17 grown in the absence of mouse fibroblasts for at least two passages using Growth Factor
18 Reduced Matrigel-coated plates (Corning). For TGFβ inhibition experiments, 20μM
19 SB431542 (Tocris) was added to the medium for the specified length of the experiment.

20 Conventional (primed) WA09/H9 (Thomson et al., 1998) were maintained in E8
21 medium as previously described (Chen et al., 2011) in DMEM/F12, 0.05% Sodium
22 Bicarbonate, 2X Insulin-Transferrin-Selenium solution (all from ThermoFisher Scientific),
23 64μg/ml L-ascorbic acid 2-phosphate (LAA) (Sigma), 1X Penicillin/Streptomycin (WT-MRC
24 Cambridge Stem Cell Institute), 25ng/ml FGF2 (Hyyönen Group, Dept of Biochemistry) and
25 2ng/ml TGFβ (BioTechne) on 10μg/ml of Vitronectin XF-coated plates (StemCell
26 Technologies) at 37°C. For TGFβ inhibition experiments, 10μM SB431542 (Tocris) was added
27 to the media for the specified length of the experiment.

28 TSCs, ETV and STB cells were generated as previously described (Dong et al., 2020)
29 with some modifications as follows. WA09/H9 NK2 naïve hPSCs were treated with 10μM
30 SB431542 (Tocris) in t2iLGö media for 5 days. Cells were dissociated with TrypLE
31 (ThermoFisher Scientific) and single cells were seeded on Collagen IV-coated plates (5μg/ml;
32 Sigma) in TSC media (Okoe et al., 2018) comprising of DMEM/F12 supplemented with
33 0.1mM β-mercaptoethanol, 0.2% FBS, 0.5% Penicillin/Streptomycin, 0.3% BSA, 1% ITS-X
34 (all from ThermoFisher Scientific), 1.5μg/ml L-ascorbic acid (Sigma), 50ng/ml EGF

1 (Peprotech), 2 μ M CHIR99021 (WT-MRC Cambridge Stem Cell Institute), 0.5 μ M A83-01
2 (Tocris), 1 μ M SB431542 (Tocris), 0.8mM VPA (Sigma), and 5 μ M Y-27632 (Cell Guidance
3 Systems) in 5% CO₂. The media was changed every two days and cells were passaged with
4 TrypLE when ~80% confluent. To induce EVT differentiation, dissociated naive-derived TSCs
5 were seeded onto plates pre-coated with 1 μ g/ml of Collagen IV (Sigma) in EVT basal media
6 comprising DMEM/F12 with 0.1mM β -mercaptoethanol, 0.5% Penicillin/Streptomycin, 0.3%
7 BSA, 1% ITS-X (all ThermoFisher Scientific), 7.5 μ M A83-01 (Tocris), 2.5 μ M Y27632 (Cell
8 Guidance Systems) and supplemented with 4% KSR (ThermoFisher Scientific) and 100ng/ml
9 NRG1 (Cell Signalling). Matrigel (Corning) was added at 2% final concentration shortly after
10 resuspending the cells in the media. On day 3, the media was replaced with EVT basal media
11 supplemented with 4% KSR (ThermoFisher Scientific), and Matrigel (Corning) was added at
12 0.5% final concentration. On day 6, the media were replaced with EVT basal medium, plus
13 0.5% Matrigel (Corning). EVTs were cultured for two more days and then collected for
14 analysis. To induce STB differentiation, dissociated TSCs were seeded in STB media
15 comprising DMEM/F12 supplemented with 0.1mM β -mercaptoethanol, 0.5%
16 Penicillin/Streptomycin, 0.3% BSA, 1% ITS-X (all ThermoFisher Scientific), 2.5 μ M Y-27632
17 (Cell Guidance Systems), 50ng/ml EGF (Peprotech), 2 μ M Forskolin (R&D) and 4% KSR
18 (ThermFisher Scientific) in ultra-low attachment plates to form cell aggregates in suspension.
19 Fresh media was added on day 3, and samples were collected for analysis on day 6.

20 Authentication of hPSCs was achieved by confirming the expression of pluripotency
21 genes and protein markers (NANOG and OCT4). Cells were routinely verified as mycoplasma-
22 free using broth and PCR-based assays. The cell lines are not on the list of commonly
23 misidentified cell lines (International Cell Line Authentication Committee).

24

25 **Western Blotting**

26 For whole cell lysates, cells were washed once in D-PBS and resuspended in ice cold RIPA
27 buffer (150mM NaCl, 50mM Tris, pH8.0, 1% NP-40, 0.5% sodium deoxycholate, 0.1%
28 sodium dodecyl sulfate) containing protease and phosphatase inhibitors for 10min. Protein
29 concentration was quantified by a BCA assay (Pierce) following the manufacturer's
30 instructions using a standard curve generated from BSA and read at 600nm on an EnVision
31 2104 plate reader. Samples were prepared by adding 4x NuPAGE LDS sample buffer
32 (ThermoFisher Scientific) plus 1% β -mercaptoethanol and heated at 95°C for 5min. 5-10 μ g of
33 protein per sample was run on a 4%–12% NuPAGE Bis-Tris Gel (ThermoFisher Scientific)
34 and then transferred to PVDF membrane by liquid transfer using NuPAGE Transfer buffer

1 (ThermoFisher Scientific). Membranes were blocked for 1hr at RT in PBS 0.05% Tween-20
2 (PBST) supplemented with 4% non-fat dried milk and incubated overnight at 4°C with primary
3 antibodies diluted in the same blocking buffer, or 5% BSA in case of phosphor-proteins. After
4 three washes in PBST, membranes were incubated for 1h at RT with horseradish peroxidase
5 (HRP)-conjugated secondary antibodies diluted in blocking buffer, then washed a further three
6 times before being incubated with Pierce ECL2 Western Blotting Substrate (ThermoFisher
7 Scientific) and exposed to X-Ray Film. Membranes were probed with antibodies in Table 1.
8 Relative quantification was performed using Fiji (ImageJ). Western blots were performed in
9 three different lines, with the NK2 line in biological duplicate (Figure 1 and Supplementary
10 Figure 1 and 3).

11

12 **RNA extraction and quantitative reverse transcription PCR (RT-qPCR)**

13 Total RNA was extracted with the GeneElute Total RNA kit (Sigma). The on-column DNase
14 digestion step was performed (Sigma) to remove any genomic DNA contamination. 500ng of
15 total RNA was used to synthesize cDNA with SuperScript II (ThermoFisher Scientific) using
16 Random primers (Promega) following manufacturer's instructions. cDNA was diluted 30-fold
17 and 2.5µl was used to perform Quantitative PCR using Kapa SYBR fast Low-Rox (Sigma) in
18 a final reaction volume of 7.5µl on a QuantStudio 5 384 PCR machine (ThermoFisher
19 Scientific). Samples were run in technical duplicate as two wells in the same qPCR plate and
20 results were analysed using *PBGD/RPLP0* as housekeeping genes. All experiments were run
21 in biological triplicate unless specified in the figure legends. Biological replicates were defined
22 as separate experiments using the same line from three different passages performed at
23 different times. All primer pairs were validated to ensure only one product was amplified and
24 with a PCR efficiency of 100% (±10%). Primer sequences used are displayed in Table 2.

25

26 **SMAD2/3 iKD line and reprogramming**

27 Validated short hairpin RNA (shRNA) sequences against SMAD2
28 (CCGGCAAGTACTCCTTGCTGGATTGCTCGAGCAATCCAGCAAGGAGTACTTGTT
29 TTTG) and SMAD3
30 (CCGGCCTCAGTGACAGCGCTATTTCTCGAGAAATAGCGCTGT
31 CACTGAGGCTTTTTG) were obtained from Sigma. Construction and transfection of the
32 sOPTiKD plasmid as well as cloning were carried out as described in (Bertero et al., 2018).
33 GeneJuice Transfection Reagent (Sigma) was used for transfection.

1 Primed SMAD2/3 inducible knockdown hPSCs were reprogrammed to a naïve state in
2 5i/LA conditions (Theunissen et al., 2014). Primed hPSCs were dissociated into single cells
3 with Accutase and 1.2 million cells per 10cm tissue culture dish were plated in primed hPSCs
4 media with 10 μ M Y-27632 (Cell Guidance Systems) onto MEF seeded at a density of 4 million
5 cells per 10cm dish. The following day, media was changed to 5i/LA comprising of a 1:1
6 mixture of DMEM/F12 and Neurobasal, 1X N-2 supplement, 1X B-27 supplement, 1%
7 nonessential amino acids, 2mM GlutaMAX, 50U/ml and 50 μ g/ml penicillin-streptomycin (all
8 from ThermoFisher Scientific), 0.1mM β -mercaptoethanol (Millipore), 50 μ g/ml bovine serum
9 albumin (ThermoFisher Scientific), 0.5% Knockout Serum Replacement (ThermoFisher
10 Scientific), 20ng/ml recombinant human LIF, 20ng/ml ActivinA, 1 μ M PD0325901 (all from
11 WT-MRC Cambridge Stem Cell Institute), 1 μ M IM-12, 1 μ M WH-4-023, 0.5 μ M SB590885
12 and 10 μ M Y-27632 (all from Cell Guidance Systems). Cells were passaged with Accutase on
13 days 5 and 10. Knockdown was induced by adding 1 μ g/ml Tetracycline (Sigma) dissolved in
14 Embryo Transfer Water (Sigma) to the media.

15

16 **Immunofluorescence**

17 Cells were grown on glass coverslips coated with either Matrigel or Vitronectin XF and fixed
18 with 4% PFA for 10min at RT, rinsed twice with PBS, and permeabilised for 20min at RT
19 using PBS/0.25% Triton X-100 (Sigma). Cells were blocked for 30min at RT with blocking
20 solution (PBS-0.25% Triton X-100 plus BSA 1%). Primary and secondary antibodies (listed in
21 Table 1) were diluted in blocking solution and incubated for 1h at 37°C. Cells were washed
22 twice with blocking solution after each antibody staining, and stained with DAPI for 5min at
23 RT (0.1 μ g/ml DAPI in PBS-0.1% Triton). Finally, coverslips were mounted on slides using
24 ProLong Gold antifade reagent (ThermoFisher Scientific) and imaged using an LSM 700
25 confocal microscope (Zeiss). To image STB cells, cell aggregates were collected by gentle
26 centrifugation (100 x g for 30sec) and fixed in 4% PFA for 20min. Cells were rinsed twice with
27 PBS and resuspended in 100 μ l of PBS and dried overnight on plus-charged slides (SuperFrost
28 Plus™ Adhesion slides, Fisher Scientific). The area containing the dried cells was circled with
29 a PAP pen and the cells were permeabilised for 5min at RT with 100 μ l of 0.1% Triton-X100
30 in PBS, and then blocked for 1h at RT with 100 μ l of 0.1% Triton-X100 plus 0.5% BSA.
31 Primary antibodies (listed in Table 1) were diluted in blocking solution and incubated overnight
32 at 4°C. Cells were washed three times with blocking solution for 5min, and stained with
33 secondary antibodies for 1h at RT. Cells were then washed for 15min with PBS, followed by
34 a second PBS wash supplemented with DAPI (0.1 μ g/ml) and a third with PBS. Finally,

1 coverslips were mounted using ProLong Gold antifade reagent (ThermoFisher Scientific) and
2 imaged using an LSM 700 confocal microscope (Zeiss). Images processed using the software
3 Fiji (ImageJ). At least four different fields from each experiment were imaged and
4 representative ones are shown in the figures.

5

6 **Chromatin immunoprecipitation (ChIP) sequencing**

7 Chromatin immunoprecipitation (ChIP) was performed as previously described (Brown et al.,
8 2011), using HEPES buffer containing 1% formaldehyde at room temperature, 10mM
9 Dimethyl 3,3'-dithiopropionimidate dihydrochloride (DTBP, Sigma) and 2.5mM 3,3'-
10 Dithiodipropionic acid di(N-hydroxysuccinimide ester) (DSP, Sigma) for the crosslinking step.
11 Experiments were performed on biological duplicates, carried out at different times with cells
12 from two different passages. 10µg of SMAD2/3 antibody (Table 1) was used per ChIP, and
13 samples were purified using the iPure v2 bead kit (Diagenode). Libraries were constructed
14 using the MicroPlex Library Preparation Kit v2 (Diagenode) following the manufacturer's
15 instructions, 10ng of input and all of the ChIP DNA was used as the starting material. Libraries
16 were quantified using KAPA Library Quantification Kit (Roche) following the manufacturer's
17 instructions and by BioAnalyser. Sequencing was performed at the Babraham Institute's Next-
18 Generation Sequencing Facility. Equimolar amounts of each library were pooled, and eight
19 samples were multiplexed on one lane of a NextSeq500 HighOutput 75bp Single End run.

20

21 Data processing

22 Reads were quality and adapter trimmed using Trim Galore! (version 0.5.0_dev, Cutadapt
23 version 1.15), and aligned to GRCh38 using Bowtie 2 (version 2.3.2).

24

25 Data analysis

26 All analyses were performed using SeqMonk ([https://www.bioinformatics.
27 babraham.ac.uk/projects/seqmonk/](https://www.bioinformatics.babraham.ac.uk/projects/seqmonk/), version 1.46.0) or R (<https://www.R-project.org/>, version
28 4.0.2). For quantitation, read lengths were extended to 300 bp and regions of coverage outliers
29 were excluded. SMAD2/3 peaks were called using a SeqMonk implementation of MACS
30 (Zhang, et. al, 2008) with parameters $p < 10E-6$, sonicated fragment size = 300. Peaks were
31 called individually for both replicates and the overlap of peaks used for annotation. Control
32 regions were randomly selected from 700 bp tiles not overlapping excluded regions.

1 Differential binding analysis was performed using the R package Diffbind, and analysis
2 of motifs that are relatively enriched in naïve compared to primed was performed using the
3 MEME suit tool AME.

4 5 **Single cell RNA-seq (10X Chromium Single Cell)**

6 H9 NK2 naïve and H9 primed hESCs were grown in presence of 20 μ M (naïve) and 10 μ M
7 (primed) of SB431542 for 7 days. Cells during the time-course were collected at day 0 (control,
8 no SB) and at day 1, 3, 5 and 7 of treatment and dissociated with Accutase (ThermoFisher
9 Scientific) for 5min at 37°C in hypoxia (5% O₂), and resuspended until single cell suspension
10 was obtained. Accutase was blocked by adding PBS/BSA 0.5% with the respective media, and
11 after a wash pellets were resuspended at a concentration of ~1,000 cells/ μ l in the respective
12 media. 3,000 cells/sample were loaded on a Chromium Chip B Single Cell following the
13 manufacturer's instruction to generate Gel Beads-in-emulsion (GEMs) using a Reagent kit v3.
14 Final Chromium Single Cell 3' Gene Expression library was generated using standard Illumina
15 paired-end constructs with P5 and P7 primers.

16
17 Data analysis

18 Cell Ranger pipeline (version 3.0.2) was used to align reads to GRCh38 assembly and generate
19 feature-barcode matrices for further gene expression analyses. Quality control, normalisation,
20 dimensionality reduction analyses and all downstream analyses were carried out using the
21 python-based library Scanpy (Wolf et al., 2018). Genes with read counts > 0 in at least 3 cells
22 and cells expressing at least 200 genes were maintained for downstream analysis. Low quality
23 cells were removed based on the percentage of unique molecular identifiers (UMIs) mapping
24 to the mitochondrial genome and the number of genes detected. Logarithmic normalisation was
25 performed, highly variable genes were selected, the total number of UMIs per cell was
26 regressed out from log-normalised data and the regressed expression values were scaled. The
27 dimensionality reduction was performed using Principal Component Analysis (PCA) and the
28 neighborhood graph of cells was calculated using the PCA representation of the scaled data
29 matrix. Clustering was performed on scaled data using the Louvain method. This graph was
30 embedded in two dimensions using Uniform Manifold Approximation and Projection
31 (UMAP).

32 Transcriptional similarity was also quantified at origin and region resolution by
33 estimating the connectivity of data manifold partitions within the partition-based graph
34 abstraction (PAGA) framework. Cluster markers and differentially expressed genes were

1 identified by applying the Wilcoxon-Rank-Sum test. In order to visualise the gradual variation
2 in the transcriptional profile following the differentiation induced by the SB treatment, cells
3 were represented as a pseudo-spatial dimension using the diffusion pseudotime method.

4 FPKM values for the ICM, EPI and TE/CTB single cell RNA-Seq datasets from (Xiang
5 et al., 2020) (GSE136447) were extracted and log₂ transformed. Similarly, log₂ reads per 10k
6 values from the first 200 cells from the A, D and E Louvain clusters were also prepared. For
7 PCA analysis the data was filtered to retain only genes which were expressed in more than
8 10% of cells in both datasets. PCA was used to separate the cells in the filtered Xiang et al.
9 data, retaining the first and second principal components. The rotations from this analysis were
10 then applied to the Louvain cluster data to project it into the same space (Figure 5e).

11 For overall correlation (Figure 5d and Supplementary Figure 5d) the mean log₂ FPKM
12 for each condition from the Xiang et al. data was correlated with the summed, log₂ FPM values
13 from the Louvain clusters using Pearson's correlation. Only genes with log₂ FPKM > 0.2 in
14 any Xiang et al. dataset and raw counts > 2 in any Louvain cluster were used for the calculation.

15 For the single cell heatmaps (Figure 5f) a Wilcoxon Rank Sum test was used to identify
16 marker genes which were significantly (fdr < 0.05, Benjamini-Hochberg correction) enriched
17 in one Xiang et al. scRNA-seq condition relative to the others. We then plotted a heatmap of
18 the expression patterns of the marker genes (columns) in each cell (rows) for both the Xiang et
19 al. and Louvain cluster data, with the cells being ordered by the group to which they belonged.
20 Measures were per-gene z-score normalised log₂ FPM.

21

22 **Data availability**

23 Sequence data that support the findings of this study have been deposited in ArrayExpress with
24 the accession numbers E-MTAB-10017 (ChIP-seq) and E-MTAB-10018 (scRNA-seq). Source
25 data files have been provided for Figure 3.

1 **Acknowledgements**

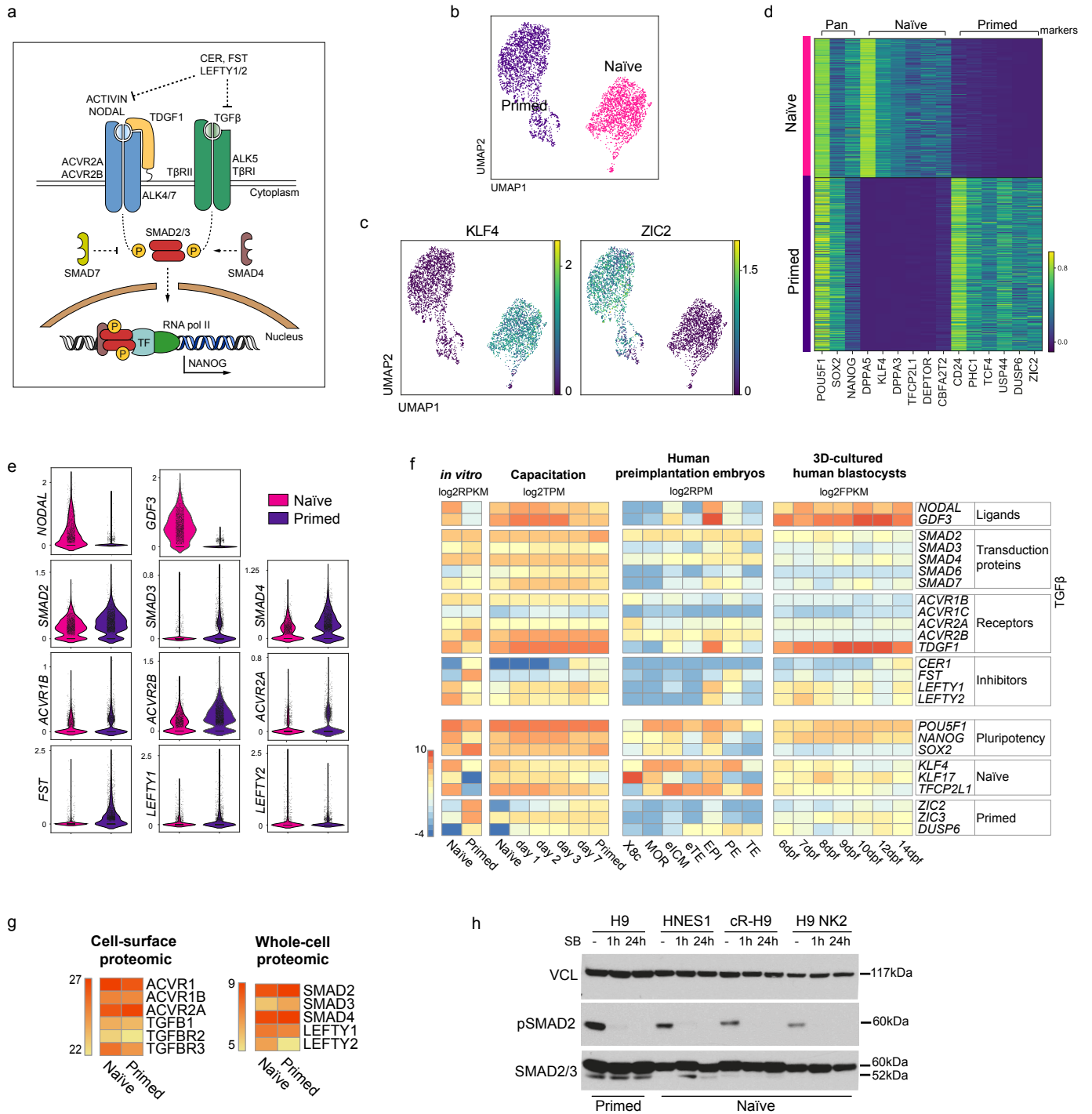
2 We thank Kristina Tabbada and Clare Murnane of the Babraham Institute Next Generation
3 Sequencing Facility, and Felix Krueger from Babraham Bioinformatics for sequencing QC and
4 mapping. We also thank Steven Leonard of the Wellcome Sanger Institute for pre-processing
5 single cell RNA-seq data. We are very grateful to Vicente Perez-Garcia (Babraham Institute
6 and the Centre for Trophoblast Research) for providing advice and reagents for characterising
7 the naïve-derived human trophoblast cells. Work in our laboratories is supported by grants
8 from the BBSRC (BBS/E/B/000C0421, BBS/E/B/000C0422) and the MRC (MR/T011769/1).
9 A.J.C. was supported by an MRC DTG Studentship (MR/J003808/1). This work was also
10 supported by the European Research Council Grant New-Chol (L.V., A.O.), the Cambridge
11 Hospitals National Institute for Health Research Biomedical Research Center (L.V., S.B.), the
12 EU H2020 INTENS grant (D.O.), Gates Cambridge PhD studentship (B.T.W.), JSPS Overseas
13 Research Fellowship (201860446) and a Grant-in-Aid (16J08005) (S.N.), and core support
14 grant from the Wellcome and Medical Research Council to the Wellcome – Medical Research
15 Council Cambridge Stem Cell Institute.

16

17 **Competing interests**

18 The authors declare no competing interests.

Figure 1

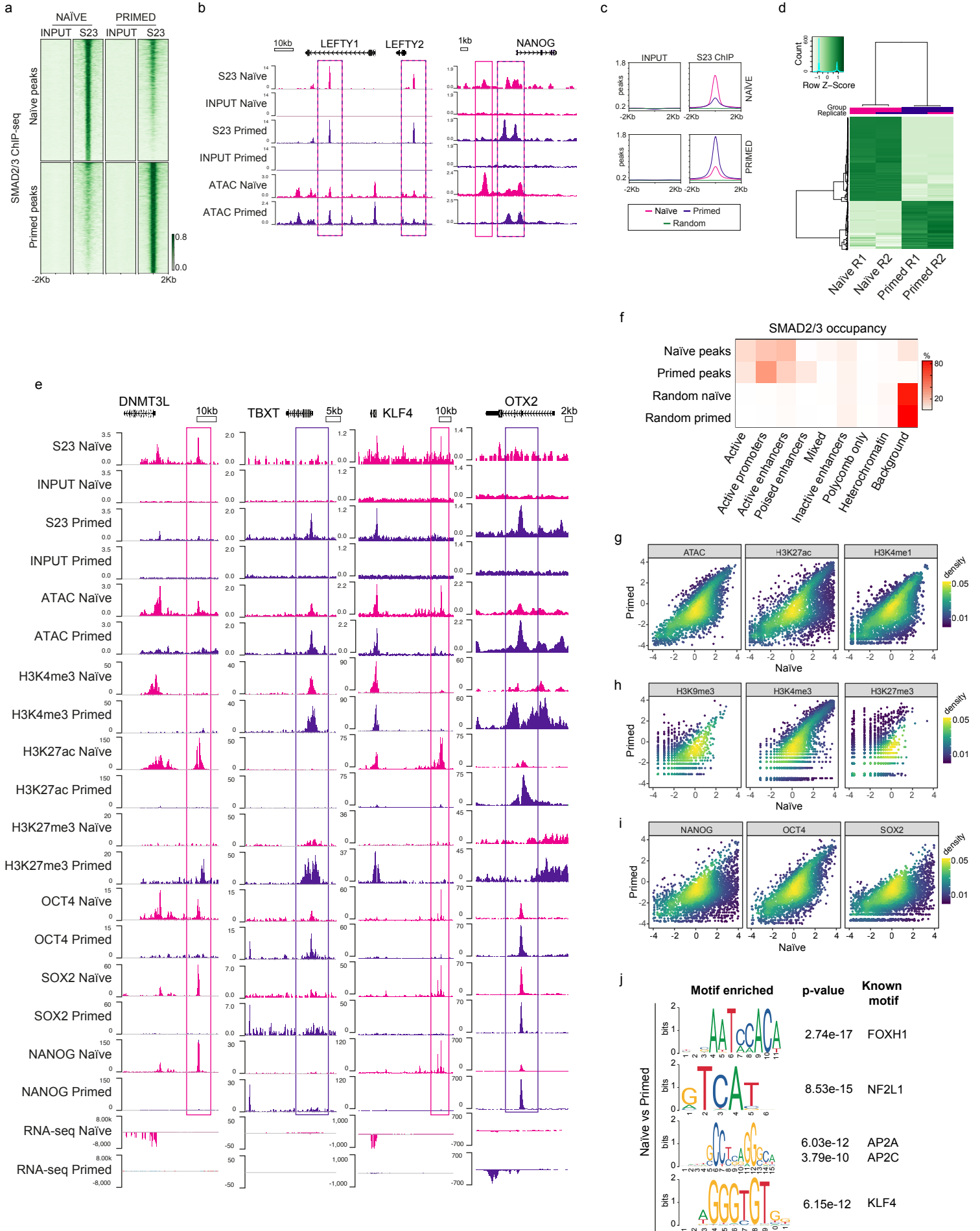


1 **Figure 1. TGF β signalling pathway is active in human naïve pluripotent stem cells**

- 2 a) Overview of the TGF β signalling pathway. Extracellular ligands ACTIVIN and NODAL
3 bind to type I (ACVR2A/2B) and type II transmembrane receptors (ALK4/7), and TGF β binds
4 to T β RI and T β RII/ALK5. NODAL requires the additional transmembrane co-receptor TDGF1
5 (CRIPTO1). The activated receptor complex phosphorylates the linker region of SMAD2 and
6 SMAD3, which enter the nucleus in complex with SMAD4. They act as transcriptional
7 regulators and induce or repress the transcription of their target loci by recruiting other
8 transcription factors (TF) and epigenetic modifiers. Several negative regulators of the
9 signalling pathway are also shown: LEFTY1/2 block the signalling pathway by binding to the
10 receptors; Cerberus (CER) and Follistatin (FST) block the ligands; SMAD7 inhibits the
11 SMAD2/3 complex.
- 12 b) 10X RNA-seq data of naïve and primed hPSCs represented on a UMAP plot.
- 13 c) UMAP visualisation of naïve and primed hPSCs reporting the relative expression of
14 respective pluripotent state markers, *KLF4* and *ZIC2*.
- 15 d) Heatmap reporting the expression values of selected naïve and primed marker genes divided
16 in pan-pluripotency markers, and naïve- and primed-specific markers within the top 250
17 differentially expressed genes.
- 18 e) Violin plots of the 10X RNA-seq data comparing the transcript expression of TGF β effectors
19 in naïve and primed hPSCs.
- 20 f) Heatmap summarising the transcript expression of TGF β effectors and pluripotency genes.
21 RNA-seq datasets shown are: *in vitro*-cultured naïve and primed hPSCs (Collier et al., 2017),
22 hPSCs undergoing naïve to primed state capacitation (Rostovskaya et al., 2019), human pre-
23 implantation embryos (Petropoulos et al., 2016), and epiblast cells within a 3D human
24 blastocyst culture system (Xiang et al., 2020). X8c: 8-cell stage; MOR: morula; eICM: early-
25 ICM; eTE: early-trophectoderm; EPI: epiblast; PE: primitive endoderm; TE: trophectoderm.
26 Dpf: days post-fertilisation.
- 27 g) Heatmaps summarising protein abundance levels determined by cell-surface proteomics
28 (Wojdyla et al., 2020) and whole cell proteomics (Di Stefano et al., 2018) for TGF β effectors
29 in naïve and primed hPSCs.
- 30 h) Western blot analysis of TGF β signalling pathway activation in H9 primed hPSCs (cultured
31 in E8 medium) and in three naïve hPSC lines cultured in t2iLGö medium: embryo-derived
32 HNES1, chemically-reset cR-H9, and transgene-reset H9 NK2. Blots show SMAD2
33 phosphorylation signal (pSMAD2-Ser465/Ser467) and total SMAD2/3 levels in normal

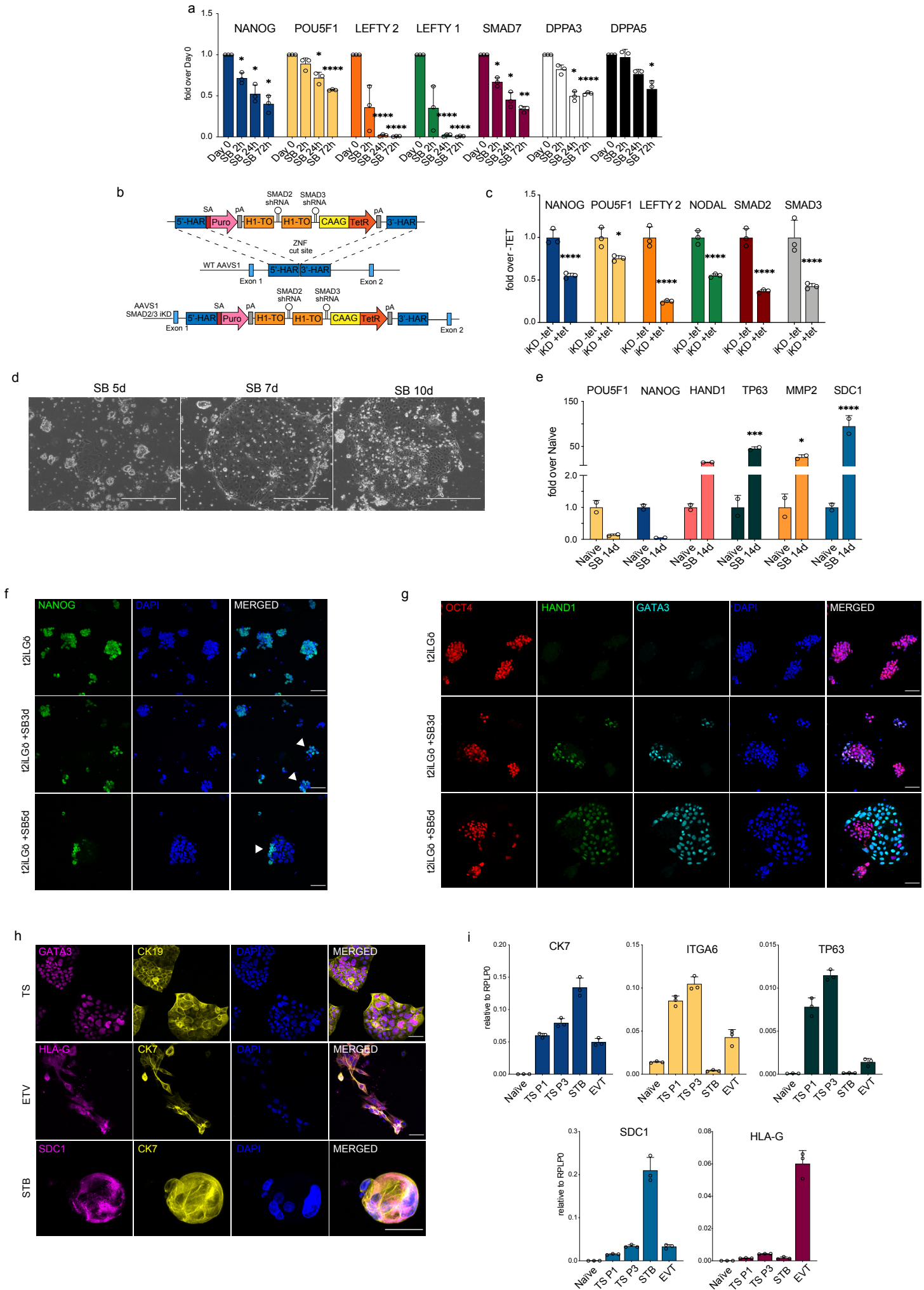
- 1 conditions (-), and following 1h and 24h of SB431542 supplementation to their culture media.
- 2 Vinculin (VCL) used as a loading control.

Figure 2



- 1 **Figure 2. SMAD2/3 binds to chromatin at common and pluripotent state-specific sites**
- 2 a) Heatmap displaying normalised SMAD2/3 (S23) ChIP-seq reads $\pm 2\text{kb}$ from the centre of
- 3 SMAD2/3-bound peaks that were independently defined in naïve (H9 NK2 line cultured in
- 4 t2iLGö medium) and primed (H9 line cultured in E8 medium) hPSCs; two biological replicates
- 5 per cell line. Top panel shows the regions identified as SMAD2/3-bound peaks in naïve cells;
- 6 lower panel shows SMAD2/3-bound peaks in primed cells.
- 7 b) Genome browser tracks reporting SMAD2/3 (S23) binding (this study) and chromatin
- 8 accessibility (ATAC-seq; Pastor et al., 2018) at the *LEFTY1/2* and *NANOG* loci in naïve and
- 9 primed hPSCs. Input tracks are shown as controls.
- 10 c) Normalised average meta-plots of SMAD2/3 (S23) ChIP signal $\pm 2\text{kb}$ from the centre of the
- 11 peaks in naïve and primed hPSCs, compared to a randomly-selected subset of regions.
- 12 d) Heatmap displaying regions that are differentially bound by SMAD2/3 in naïve and primed
- 13 hPSCs in two biological replicates (R1 and R2).
- 14 e) Genome browser tracks reporting expression (RNA-seq), chromatin accessibility (ATAC-
- 15 seq), and ChIP-seq datasets of SMAD2/3 (S23), histone marks for enhancers (H3K27ac) and
- 16 promoters (H3K4me3, H3K27me3), and transcription factors (OCT4, SOX2, NANOG) at the
- 17 *DNMT3L*, *TBXT*, *KLF4*, *OTX2* loci. Input tracks are shown as controls. The following data sets
- 18 are shown: ATAC-seq (Pastor et al., 2018); H3K4me3 (Theunissen et al., 2014); H3K4me1
- 19 (Chovanec et al., 2021; Gifford et al., 2013); H3K27me3 (Theunissen et al., 2014); H3K27ac
- 20 (Ji et al., 2016); OCT4 (Ji et al., 2016); SOX2 (Chovanec et al., 2021); NANOG (Chovanec et
- 21 al., 2021; Gifford et al., 2013) and RNA-seq (Takashima et al., 2014).
- 22 f) Heatmap showing the frequency of SMAD2/3 peak centre locations with respect to
- 23 ChromHMM states in naïve and primed hPSCs (Chovanec et al., 2021). SMAD2/3 peaks in
- 24 naïve and primed hPSCs were annotated with their respective ChromHMM states. The
- 25 annotations associated with the randomly-selected control regions reflect the overall genomic
- 26 representation of chromatin states.
- 27 g-i) Density coloured scatter plots showing indicated ChIP-seq and ATAC-seq values (\log_2
- 28 RPM) in naïve versus primed hPSCs. Each dot corresponds to one naïve-specific SMAD2/3
- 29 peak.
- 30 j) Differential motif enrichment reporting the top four motifs (ranked by p-value) at SMAD2/3
- 31 binding sites in naïve hPSCs that are enriched compared to motifs identified at SMAD2/3
- 32 binding sites in primed hPSCs.

Figure 3

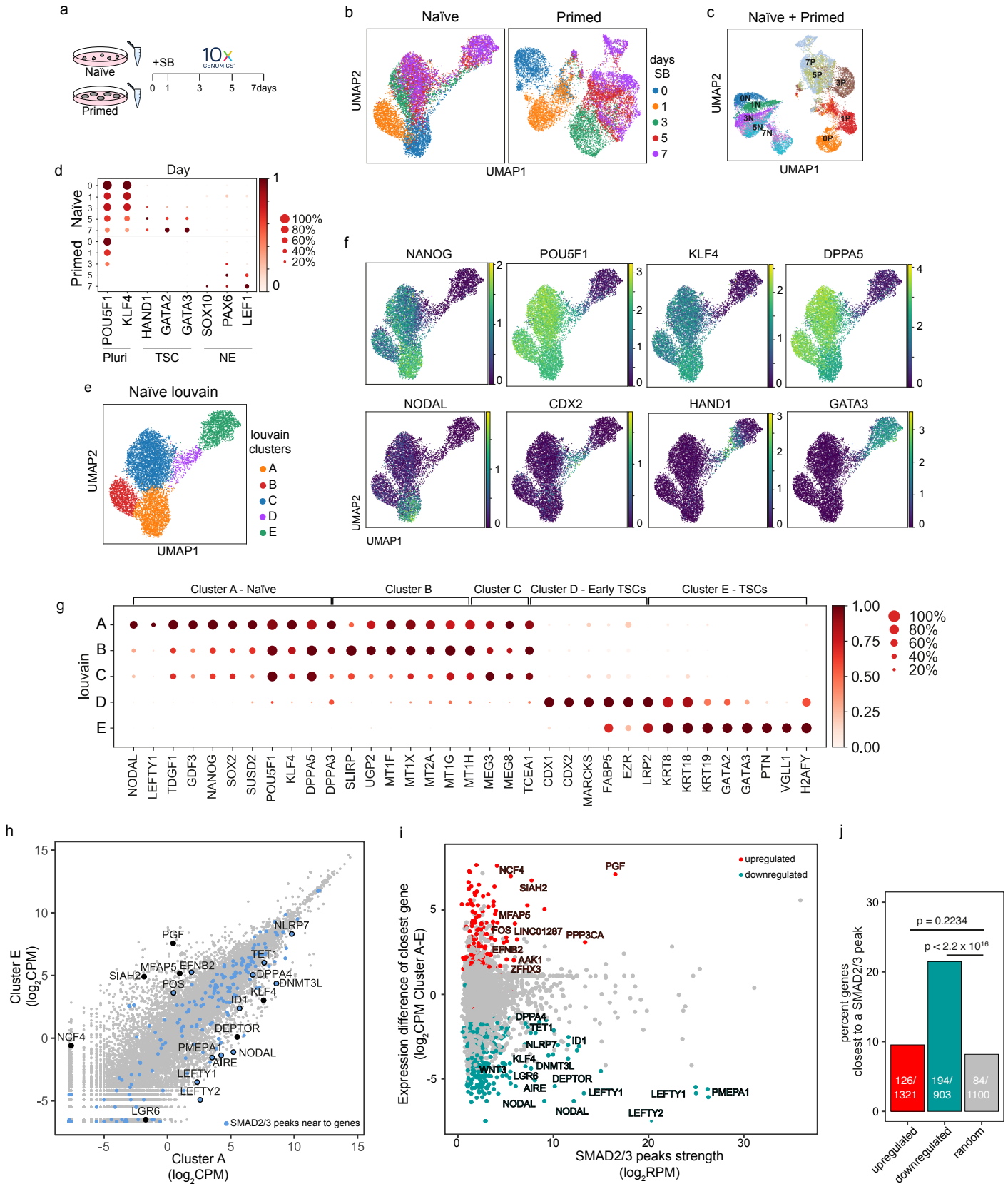


1 **Figure 3. Inhibiting TGF β signalling induces loss of pluripotency in naïve hPSCs**

- 2 a) RT-qPCR expression analysis of pluripotency-associated genes and TGF β -associated genes
3 in naïve hPSCs (H9 NK2 line) following SB431542 treatment (t2iLGö + SB). Expression
4 levels are shown as fold changes relative to day 0.
- 5 b) Schematic showing the integration of a single-step optimised inducible knock-down
6 targeting construct into the *A/VSI* locus of H9 hPSCs, enabling the expression of SMAD2 and
7 SMAD3 short hairpin RNAs (shRNAs) under the control of a tetracycline inducible promoter.
8 ZFN: zinc-finger nucleases; 5'-HAR/3'-HAR: upstream/downstream homology arm; H1-TO:
9 Tetracycline-inducible H1 Pol III promoter carrying one tet operon after the TATA box;
10 CAAG: CMV early enhancer, chicken β -actin and rabbit β -globin hybrid promoter; TetR:
11 Tetracycline-sensitive repressor protein; SA: splice acceptor; Puro, Puromycin resistance; pA,
12 polyadenylation signal. Schematic adapted from (Bertero et al., 2016).
- 13 c) RT-qPCR analysis of gene expression levels in SMAD2/3 inducible knock-down (iKD) H9
14 naïve hPSCs following 5 days of tetracycline (tet) treatment. Expression levels are shown for
15 each gene as fold change relative to iKD -tet. Cells were cultured in t2iLGö medium.
- 16 d) Phase contrast pictures of H9 NK2 naïve hPSCs after 5, 7, and 10 days of SB treatment in
17 t2iLGö medium. Scale bars: 400 μ m.
- 18 e) RT-qPCR analysis of trophoblast (*HAND1*, *TP63*, *MMP2* and *SDC1*) and pluripotency
19 (*POU5F1*, *NANOG*) gene expression levels in naïve hPSCs following long term (14 days) SB
20 treatment in t2iLGö medium. Expression levels are shown as fold changes relative to day 0
21 samples, n = 2 biological replicates.
- 22 f) Immunofluorescence microscopy showing the downregulation of NANOG (green) in naïve
23 hPSCs following 3 and 5 days of SB treatment. DAPI signal in blue. White arrowheads indicate
24 colonies displaying heterogeneous expression of NANOG. Scale bars: 50 μ m.
- 25 g) Immunofluorescence microscopy for OCT4 (red), HAND1 (green), GATA3 (cyan) and
26 DAPI (blue) in naïve hPSCs following 3 and 5 days of SB treatment in t2iLGö medium. Scale
27 bars: 50 μ m.
- 28 h) Immunofluorescence microscopy for GATA3, HLA-G, SDC1 (magenta), CK19 and CK7
29 (yellow), and DAPI (blue) in naïve-derived trophoblast stem cells (TS), extravillous
30 trophoblast (ETV) and syncytiotrophoblast (STB). Scale bars: 50 μ m.
- 31 i) RT-qPCR analysis of gene expression levels in naïve-derived trophoblast stem cells (TS),
32 extravillous trophoblast (ETV) and syncytiotrophoblast (STB) compared to undifferentiated
33 naïve hPSCs. Expression levels are shown for each gene relative to the housekeeping gene
34 *RPLP0*.

- 1 RT-qPCR data show the mean \pm SD of three biological replicates (unless specified otherwise)
- 2 and were compared to their relative control using an ANOVA with Tukey's or Šídák's multiple
- 3 comparisons test (* $p \leq 0.05$, ** $p \leq 0.01$, *** $p \leq 0.001$, **** $p \leq 0.0001$). See also Figure 3–
- 4 Source Data 1.

Figure 4

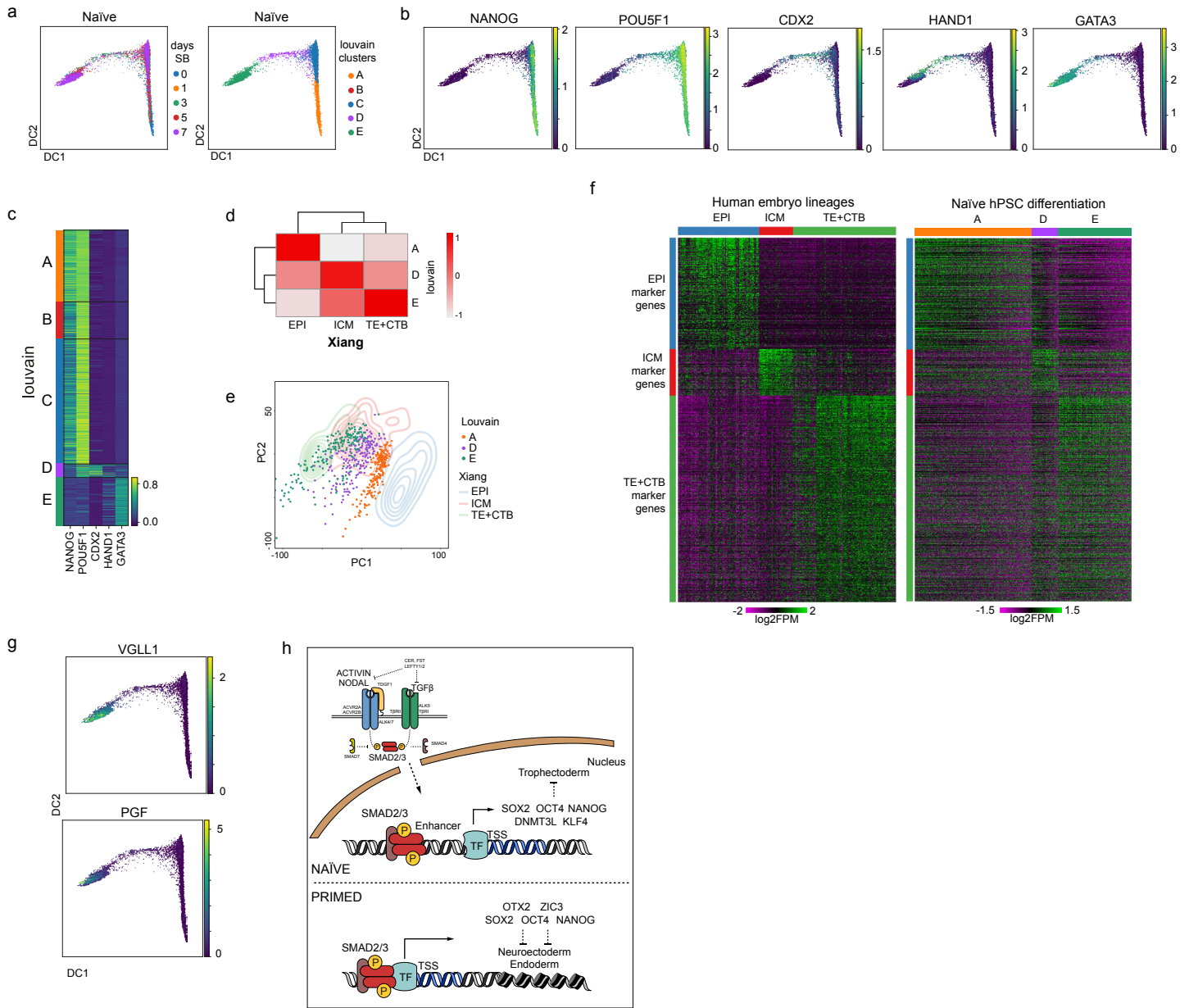


1 **Figure 4. Single-cell transcriptional analysis reveals a trophoblast-like population arising**
2 **in response to TGF β inhibition in naïve hPSCs**

- 3 a) Overview of the experimental procedure. Naïve and primed hPSCs were cultured in the
4 presence of SB-431542 (SB), a potent TGF β inhibitor, and samples were collected at days 0,
5 1, 3, 5 and 7. Single cell transcriptomes were obtained by 10X sequencing.
- 6 b) UMAP visualisation of naïve and primed cells during the SB time-course experiment,
7 separated by days of treatment.
- 8 c) UMAP visualisation of the combined naïve and primed data set, separated by days of SB
9 treatment (indicated by the number in the labels). N, naïve; P, primed.
- 10 d) Dot plot of selected gene expression values in naïve and primed cells during the SB time-
11 course experiment, plotted by days of treatment (in rows). Each dot represents two values:
12 mean expression within each category (visualised by colour) and fraction of cells expressing
13 the gene (visualised by the size of the dot). Genes are indicative of pluripotent cells (Pluri),
14 trophoblast stem cells (TSC) and neuroectoderm cells (NE).
- 15 e) UMAP visualisation of naïve hPSCs during the SB time-course experiment, separated by
16 Louvain clustering (five clusters, A to E).
- 17 f) UMAP visualisation of naïve cells during the SB time-course experiment, showing the
18 relative expression of pluripotency markers, *NANOG*, *POU5F1*, *KLF4*, and *DPPA5*; TGF β
19 effectors, *NODAL*; and trophoblast markers, *CDX2*, *HAND1*, *GATA3*.
- 20 g) Dot plot of expression values in naïve cells during the SB time-course experiment, separated
21 by the five Louvain clusters. The genes shown represent a subset of the top 25 differentially
22 expressed genes between the five clusters, as reported in Figure supplement 5e. Each dot
23 represents two values: mean expression within each category (visualised by colour) and
24 fraction of cells expressing the gene (visualised by the size of the dot).
- 25 h) Scatter plot reporting pseudobulk RNA-seq values (from 10X data) for cells in Louvain
26 clusters A and E. Each dot represents one gene. Genes that have SMAD2/3 ChIP-seq peaks
27 (\log_2 RPM > 5) within 12 kb of their transcription start site (TSS) are highlighted in blue and
28 annotated. Several differentially expressed genes that are the closest gene to a SMAD2/3 peak
29 (but are further away than 12 kb) are also named.
- 30 i) Scatter plot showing SMAD2/3 ChIP-seq peak strength (\log_2 RPM) versus the expression
31 difference (cluster A – cluster E; \log_2 CPM) of the gene nearest to the SMAD2/3 peak.
32 Upregulated genes, red; downregulated genes, green.
- 33 j) SMAD2/3 peaks were annotated with their nearest genes. Bar plot showing the percentage
34 of genes that are the closest gene to a SMAD2/3 peak for genes that are upregulated (red) or

1 downregulated (green) between cells in clusters A and E. A randomly-selected set of control
2 genes are shown in grey. The number of closest genes and the set size are reported within the
3 bars. Statistical testing was performed using Chi-square test with Yates continuity and
4 Bonferroni multiple testing correction.

Figure 5



1 **Figure 5. Differentiation of TGF β -inhibited naïve hPSCs transcriptionally recapitulates**
2 **early trophoderm specification in human embryos**

3 a) Diffusion maps of naïve cells during the SB time-course experiment, separated by days of
4 treatment (left) and Louvain clustering (right).

5 b) Overlay of the diffusion maps with the relative expression of pluripotency markers *NANOG*,
6 and *POU5F1*, and trophoblast markers *CDX2*, *HAND1*, *GATA3*.

7 c) Heatmap of the expression values of genes reported in Figure 5b separated by the Louvain
8 clusters. Note the overlap in the expression of pluripotency and trophoblast markers in cells
9 within cluster D.

10 d) Correlation plot between pseudobulk data from Louvain clusters A/D/E and EPI (Epiblast),
11 ICM (Inner Cell Mass), and TE+CTB (Trophoderm+Cytotrophoblast) from cultured human
12 pre-gastrulation embryos (Xiang et al., 2020).

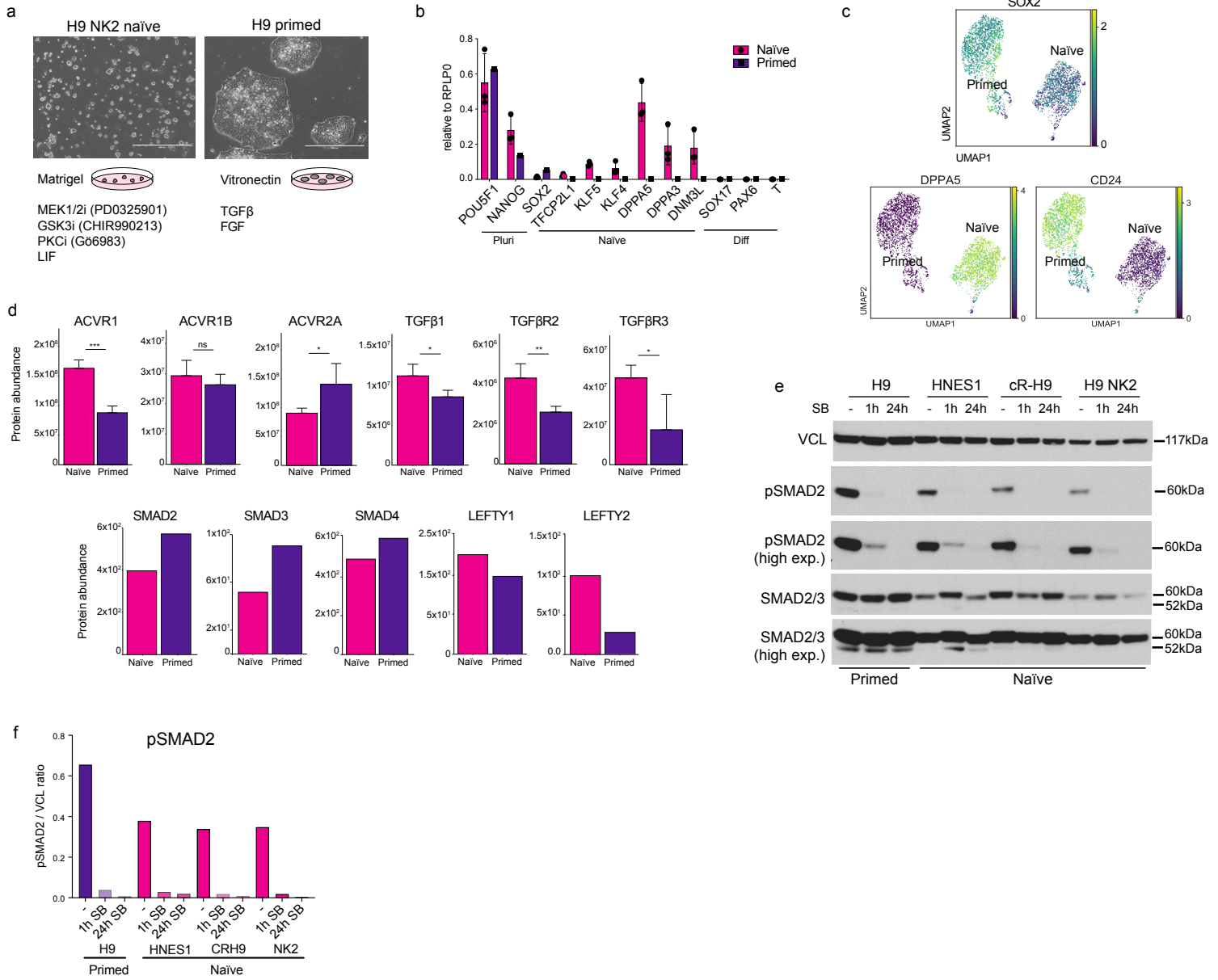
13 e) PCA plot overlapping 200 randomly-selected cells from each of the Louvain clusters A/D/E
14 (individual dots) and data from 3D-cultured human pre-gastrulation embryos (Xiang et al.,
15 2020), based on EPI, ICM and TE+CTB cells (contour lines). PC1 variance 2.15, PC2 variance
16 1.41.

17 f) Heatmaps visualising the expression of genes in EPI, ICM and TE+CTB (Xiang et al., 2020)
18 and cells in Louvain clusters A/D/E. Note that the genes are in the same order for both plots.

19 g) Diffusion maps of naïve cells during the SB time-course experiment showing the relative
20 expression of CTB markers – *VGLL1* and *PGF*.

21 h) We propose there is a continuum of TGF β /Activin/Nodal signalling that spans a
22 developmental window of human pluripotent states from naïve to primed. In both states, active
23 TGF β signalling promotes the expression of common pluripotency genes, such as *NANOG* and
24 *POU5F1*, and contributes to the maintenance of pluripotency. SMAD2/3 are additionally
25 required in naïve hPSCs to sustain the expression of naïve pluripotency factors, including *KLF4*
26 and *DNMT3L*. Inactivating TGF β signalling in naïve hPSCs leads to the downregulation of
27 pluripotency genes, thereby enabling the induction of trophoblast differentiation.

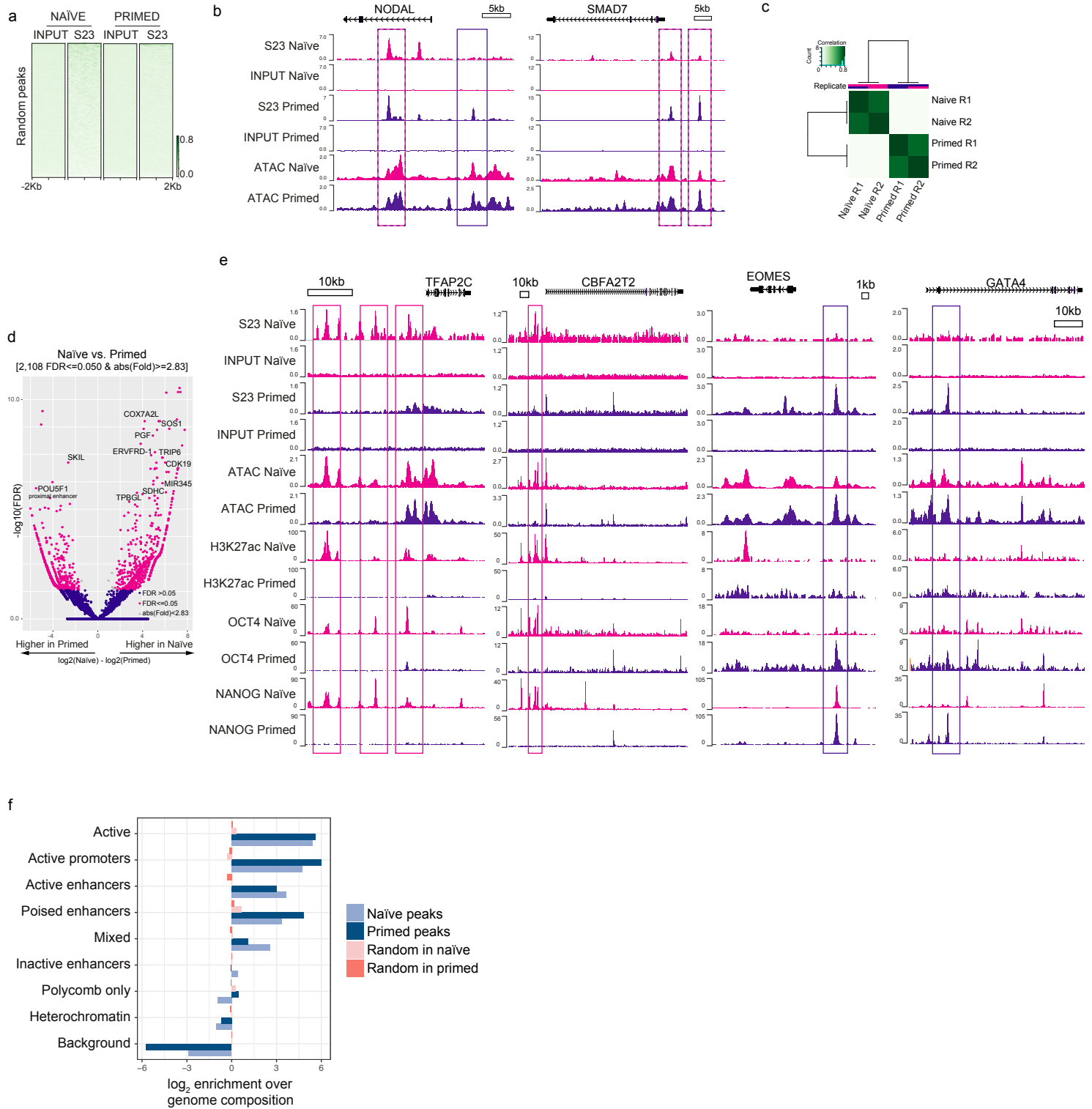
Supplemental Figure 1



1 **Supplemental Figure 1. Validation of naïve and primed hPSCs and TGF β signalling**
2 **pathway activation**

- 3 a) Overview of the conditions used for culturing naïve and primed hPSCs and representative
4 phase-contrast images.
- 5 b) RT-qPCR expression analysis of pan-pluripotency genes (Pluri), naïve markers (Naïve) and
6 early-stage germ cell layer markers (Diff) in naïve and primed hPSCs. Data show the mean \pm
7 SD of three biological replicates, relative to the housekeeping gene *RPLP0*.
- 8 c) UMAP visualisation of naïve and primed cells reporting the relative expression of
9 pluripotency marker *SOX2*, naïve marker *DPPA5*, and primed marker *CD24*.
- 10 d) Protein abundance levels for several TGF β receptors (upper; (Wojdyla et al., 2020)) and
11 transduction proteins (lower; (Di Stefano et al., 2018)) in naïve and primed hPSCs. The upper
12 charts show the mean \pm SD of three (naïve) or four (primed) biological replicates and were
13 compared using a LIMMA-moderated t test with Benjamini-Hochberg correction (ns, $q > 0.05$,
14 $*q < 0.05$, $**q < 0.01$, $***q < 0.001$, $****q < 0.0001$). The lower charts show protein
15 abundance of one biological replicate per cell type.
- 16 e) Expanded western blot from Figure 1h comparing TGF β pathway activation in primed H9
17 cells (cultured in E8 medium) and in three naïve hPSC lines cultured in t2iLGö medium:
18 embryo-derived HNES1, chemically-reset cR-H9, and transgene-reset H9 NK2 naïve cells.
19 Blots show SMAD2 phosphorylation signal and total SMAD2/3 in normal conditions (-), and
20 following 1h and 24h of SB431542 supplementation to their culture media. Two separate
21 exposures are shown. Vinculin (VCL) used as loading control.
- 22 f) Relative quantification of western blot from Figure 1h performed using the software Fiji
23 (ImageJ) reporting the pSMAD2 / Vinculin (VCL) ratio.

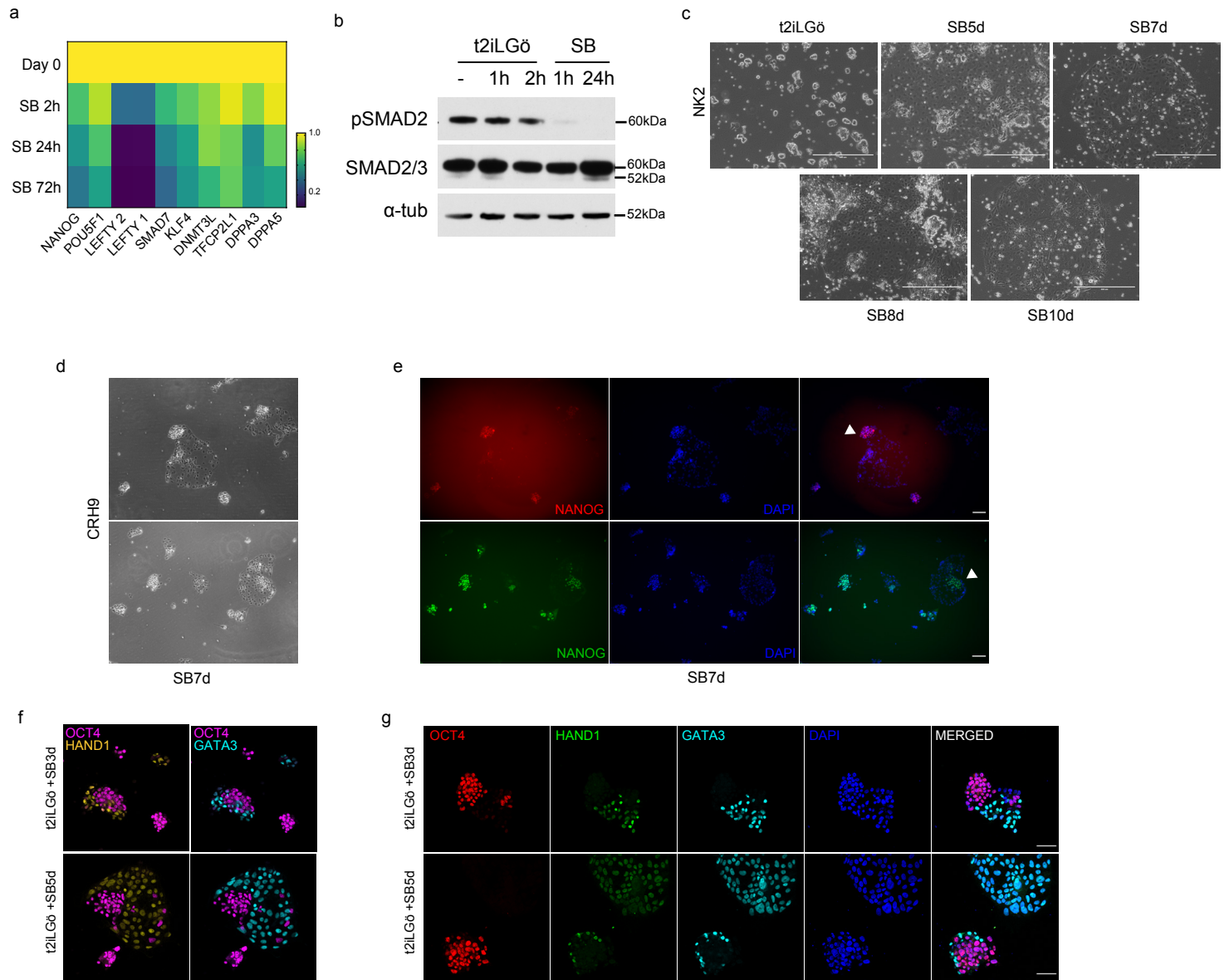
Supplemental Figure 2



1 **Supplemental Figure 2. SMAD2/3 binds to chromatin at common and state-specific sites**

- 2 a) Heatmap displaying normalised SMAD2/3 ChIP-seq signal ± 2 kb from the centre of the
3 peaks in a randomly-selected subset of regions, complementing Figure 2a.
- 4 b) Genome browser tracks overlapping SMAD2/3 (S23) binding sites in naïve and primed cells
5 with chromatin accessibility (ATAC-seq) at the *NODAL* and *SMAD7* loci. Input is shown as
6 control.
- 7 c) Correlation heatmap reporting the clustering of SMAD2/3 ChIP-seq replicates (R1 and R2)
8 for each cell type, based on the count scores.
- 9 d) Volcano plot reporting the fold change in SMAD2/3 ChIP-seq signal at SMAD2/3 peaks
10 between naïve and primed cells and the associated false discovery rate. Each dot represents a
11 SMAD2/3 peak. Dots highlighted in pink are significantly differentially bound sites (\log_{10} FDR
12 ≤ 0.05 ; \log_2 fold changes ≥ 1.5).
- 13 e) Genome browser tracks exemplify the overlap between SMAD2/3 (S23) ChIP-seq binding
14 sites in naïve and primed cells with chromatin accessibility (ATAC-seq), histone marks for
15 active enhancers (H3K27ac), and OCT4 and NANOG ChIP-seq signal. Input is shown as
16 control.
- 17 f) Bar plot reporting the \log_2 enrichment of SMAD2/3 peaks at ChromHMM-defined promoter
18 and enhancer regions compared to other genomic regions. Related to Figure 2f.

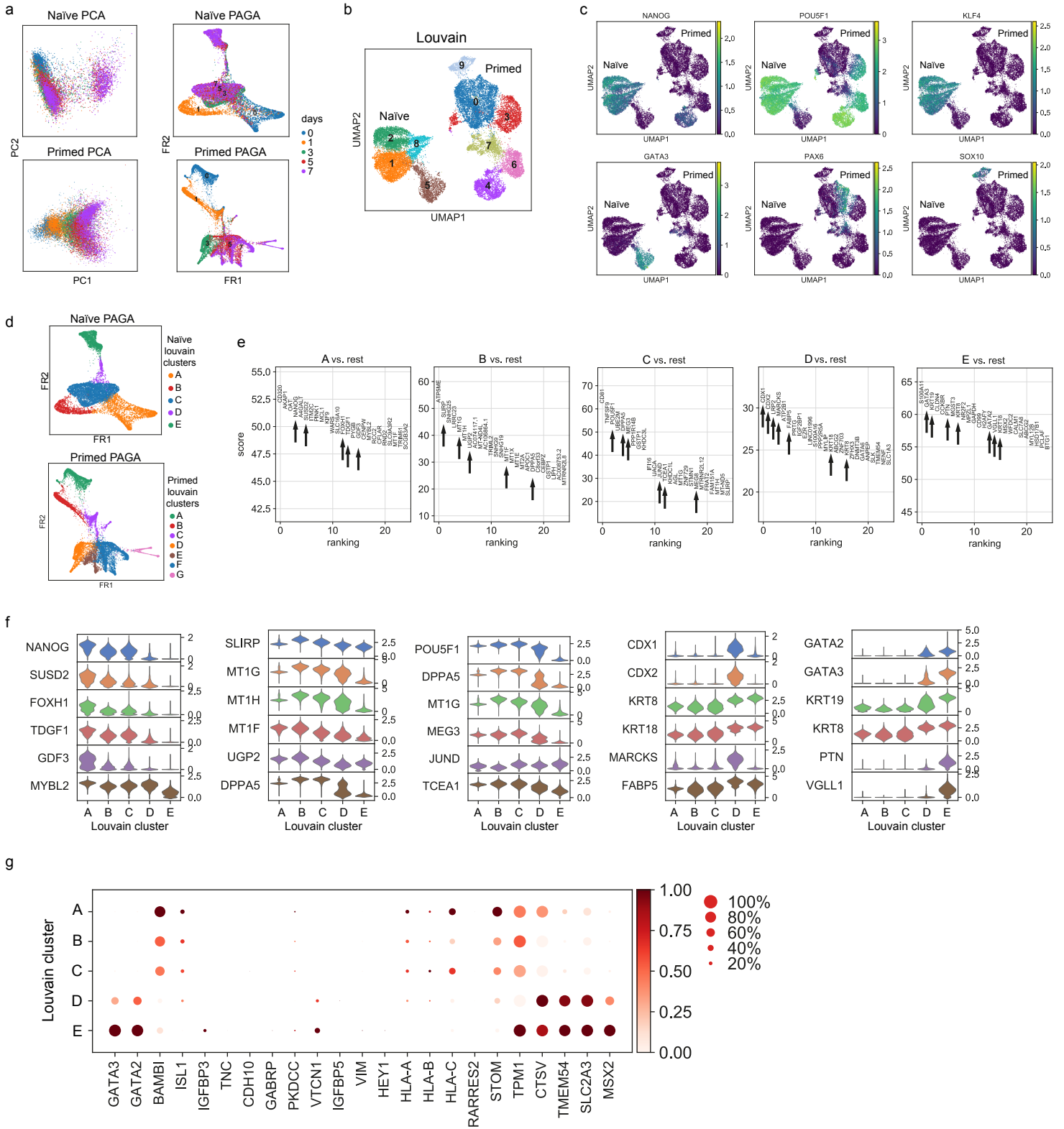
Supplemental Figure 3



1 **Supplemental Figure 3. TGF β signalling inhibition induces loss of pluripotency in**
2 **different naïve hPSCs**

- 3 a) Heatmap reporting RT-qPCR expression analysis of pluripotency genes and TGF β -
4 associated genes in naïve cells following the addition of SB to the culture medium (t2iLGö),
5 related to Figure 3a. Data show the mean of three biological replicates as fold changes
6 compared to day 0.
- 7 b) Western blot showing TGF β pathway activation in H9 NK2 naïve cells through the
8 phosphorylation of SMAD2 (pSMAD2) and also total SMAD2/3 in normal conditions (-), after
9 1h and 2h of fresh media change (t2iLGö), and following 1h and 24h of SB treatment
10 (t2iLGö+SB). Alpha-tubulin (α -tub) used as loading control.
- 11 c) Phase-contrast images of H9 NK2 naïve cells at day 0 (t2iLGö) and following 5, 7, 8 and 10
12 days of SB supplementation to the t2iLGö medium. Scale bars: 400 μ m.
- 13 d) Phase-contrast images of chemically-reset cR-H9 naïve cells after 7 days of SB treatment.
- 14 e) Immunofluorescence microscopy of H9 NK2 naïve hPSCs for NANOG (red/green), and
15 DAPI (blue), after 7 days of SB treatment in chemically-reset cR-H9 naïve cells, matching the
16 phase-contrast images in Supplementary Figure 3d. White arrowheads indicate colonies
17 displaying heterogeneous NANOG expression. Scale bars: 50 μ m.
- 18 f) Immunofluorescence microscopy complementing Figure 3g showing (left) OCT4 (red) and
19 HAND1 (green) overlap, or (right) OCT4 (red) and GATA3 (cyan) overlap after 3 and 5 days
20 of SB treatment. Scale bars: 50 μ m.
- 21 g) Immunofluorescence microscopy of H9 NK2 naïve hPSCs for OCT4 (red), HAND1 (green),
22 GATA3 (cyan) and DAPI (blue) after 3 (upper) and 5 (lower) days of SB treatment. Scale bars:
23 50 μ m.

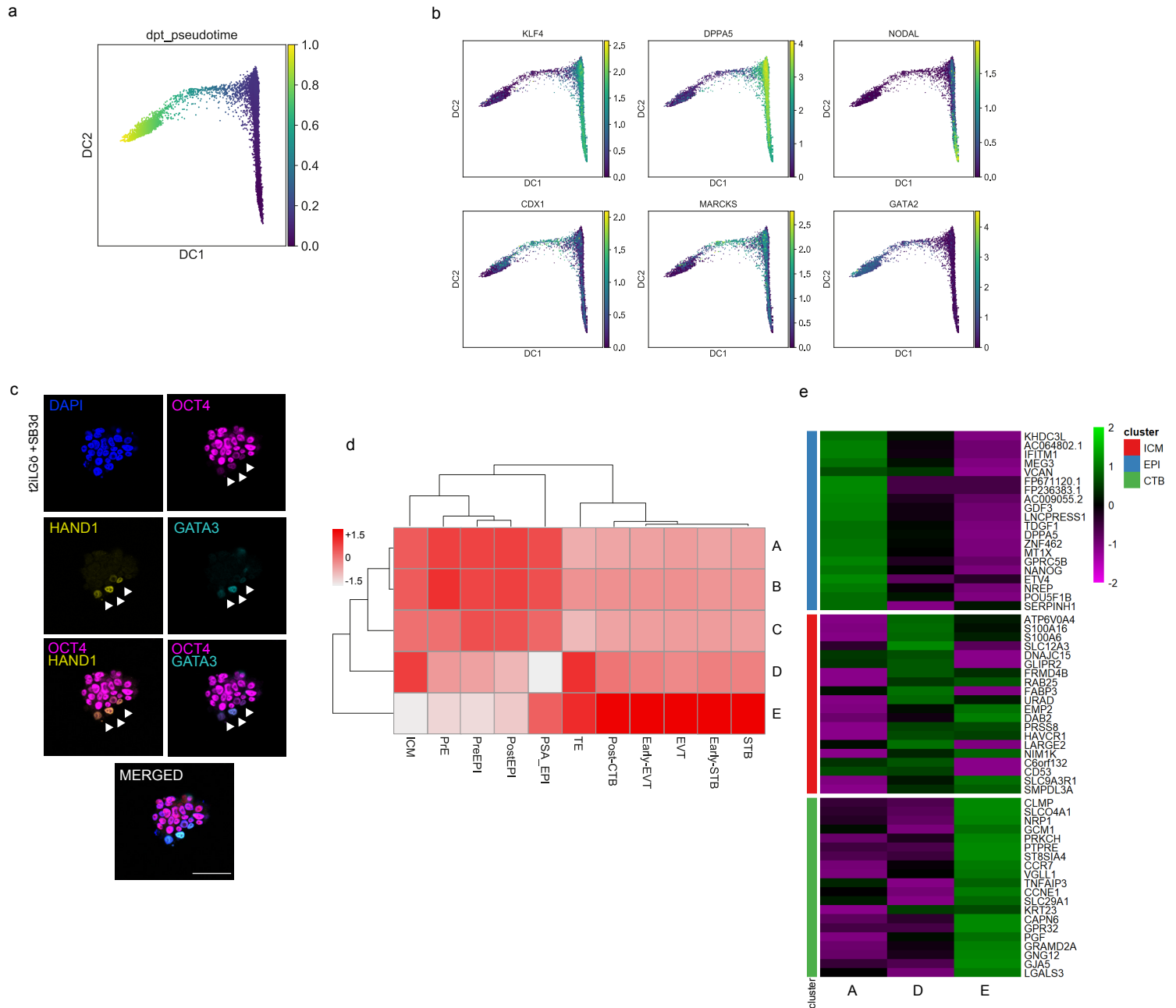
Supplemental Figure 4



1 **Supplemental Figure 4. Single-cell transcriptional analysis reveals different trajectories**
2 **between naïve and primed hPSCs following TGFβ inhibition**

- 3 a) PCA and partition-based graph abstraction (PAGA) connectivity visualisation of the 10X
4 RNA-seq data in naïve and primed hPSCs during the SB time-course, separated by days of
5 treatment.
- 6 b) UMAP visualisation of the combined naïve and primed cell 10X dataset during the SB time-
7 course experiment, separated by Louvain clustering.
- 8 c) UMAP visualisation of the combined naïve and primed cell 10X dataset reporting the
9 relative expression of pluripotency markers *NANOG*, *POU5F1*, *KLF4*, trophoblast marker
10 *GATA3*, and neuroectoderm markers *PAX6*, *SOX10*.
- 11 d) PAGA connectivity visualisation of naïve and primed cells during the SB time-course
12 experiment, separated by Louvain clustering.
- 13 e) Summarised results showing the top 25 differentially expressed genes between Louvain
14 clusters, identified by applying a Wilcoxon-Rank-Sum test. Black arrows highlight informative
15 genes relative to each cluster.
- 16 f) Violin plots reporting the expression of a subset of genes identified in Figure 4g and
17 Supplementary Figure 4e.
- 18 g) Dot plot of expression values in naïve cells during the SB time-course experiment, separated
19 by the five Louvain clusters. The genes shown represent a subset of amnion marker genes
20 reported in (Guo et al., 2021; Io et al., 2021; Zhao et al., 2021). Note that some genes are also
21 expressed in trophoblast cells. Each dot represents two values: mean expression within each
22 category (visualised by colour) and fraction of cells expressing the gene (visualised by the size
23 of the dot).

Supplemental Figure 5



1 **Supplemental Figure 5. Pseudotime trajectories of TGF β -inhibited naïve hPSCs**
2 **recapitulates early trophoderm specification in human embryos**

3 a) Diffusion maps of naïve hPSC 10X scRNA-seq data during the SB time-course, reporting
4 diffusion pseudotime scores.

5 b) Diffusion map visualisation of naïve cells during the SB time-course reporting the relative
6 expression of additional pluripotency markers *KLF4* and *DPPA5*, TGF β effector *NODAL*, and
7 trophoblast markers *CDX1*, *MARCKS* and *GATA2*.

8 c) Immunofluorescence microscopy for OCT4 (red), HAND1 (green), GATA3 (cyan) and
9 DAPI (blue) in H9 NK2 naïve cells following 3 days of SB supplementation to t2iLGö medium.
10 White arrowheads indicate cells that co-express low levels of OCT4 and HAND1 or GATA3.
11 Scale bars: 50 μ m.

12 d) Correlation heatmap between the pseudobulked datasets from all Louvain clusters
13 (A/B/C/D/E) and the identified cell lineages from the cultured human pre-gastrulation embryos
14 (Xiang et al., 2020). CTB: Cytotrophoblast; ETV: Extravillous trophoblast; STB:
15 Syncytiotrophoblast; EPI: Epiblast; ICM: Inner Cell Mass; PrE: Primitive Endoderm, TE:
16 Trophoderm.

17 e) Heatmap reporting the expression in the Louvain clusters A, D, and E of the top 20
18 differentially expressed genes between EPI, ICM and CTB cell lineages (based on data
19 published by (Xiang et al., 2020).

1 References

- 2 Alici-Garipcan A, Özçimen B, Süder I, Ülker V, Önder TT, Özören N. 2020. NLRP7 plays a
3 functional role in regulating BMP4 signaling during differentiation of patient-derived
4 trophoblasts. *Cell Death Dis* **11**:658.
- 5 Azuara V, Perry P, Sauer S, Spivakov M, Jørgensen HF, John RM, Gouti M, Casanova M, Warnes G,
6 Merckenschlager M, Fisher AG. 2006. Chromatin signatures of pluripotent cell lines. *Nat Cell*
7 *Biol* **8**:532–538.
- 8 Barakat TS, Halbritter F, Zhang M, Rendeiro AF, Perenthaler E, Bock C, Chambers I. 2018.
9 Functional Dissection of the Enhancer Repertoire in Human Embryonic Stem Cells. *Cell Stem*
10 *Cell* **23**:276–288.e8.
- 11 Battle SL, Doni Jayavelu N, Azad RN, Hesson J, Ahmed FN, Overbey EG, Zoller JA, Mathieu J,
12 Ruohola-Baker H, Ware CB, Hawkins RD. 2019. Enhancer Chromatin and 3D Genome
13 Architecture Changes from Naive to Primed Human Embryonic Stem Cell States. *Stem Cell*
14 *Reports* **12**:1129–1144.
- 15 Bayerl J, Ayyash M, Shani T, Manor YS, Gafni O, Massarwa R, Kalma Y, Aguilera-Castrejon A,
16 Zerbib M, Amir H, Sheban D, Geula S, Mor N, Weinberger L, Naveh Tassa S, Krupalnik V,
17 Oldak B, Livnat N, Tarazi S, Tawil S, Wildschutz E, Ashouokhi S, Lasman L, Rotter V, Hanna
18 S, Ben-Yosef D, Novershtern N, Viukov S, Hanna JH. 2021. Principles of signaling pathway
19 modulation for enhancing human naive pluripotency induction. *Cell Stem Cell*.
20 doi:10.1016/j.stem.2021.04.001
- 21 Bernstein BE, Mikkelsen TS, Xie X, Kamal M, Huebert DJ, Cuff J, Fry B, Meissner A, Wernig M,
22 Plath K, Jaenisch R, Wagschal A, Feil R, Schreiber SL, Lander ES. 2006. A bivalent chromatin
23 structure marks key developmental genes in embryonic stem cells. *Cell* **125**:315–326.
- 24 Bertero A, Pawlowski M, Ortmann D, Snijders K, Yiangou L, de Brito MC, Brown S, Bernard WG,
25 Cooper JD, Giacomelli E, Gambardella L, Hannan NRF, Iyer D, Sampaziotis F, Serrano F,
26 Zonneveld MCF, Sinha S, Kotter M, Vallier L. 2016. Optimized inducible shRNA and
27 CRISPR/Cas9 platforms for in vitro studies of human development using hPSCs. *Development*.
28 doi:10.1242/dev.138081
- 29 Bertero A, Yiangou L, Brown S, Ortmann D, Pawlowski M, Vallier L. 2018. Conditional
30 Manipulation of Gene Function in Human Cells with Optimized Inducible shRNA. *Curr Protoc*
31 *Stem Cell Biol* **44**:5C.4.1–5C.4.48.
- 32 Blakeley P, Fogarty N, Del Valle I, Wamaitha S, Hu TX, Elder K, Snell P, Christie L, Robson P,
33 Niakan K. 2017. Defining the three cell lineages of the human blastocyst by single-cell RNA-
34 seq. *Mechanisms of Development*. doi:10.1016/j.mod.2017.04.015
- 35 Bredenkamp N, Stirparo GG, Nichols J, Smith A, Guo G. 2019a. The Cell-Surface Marker Sushi
36 Containing Domain 2 Facilitates Establishment of Human Naive Pluripotent Stem Cells. *Stem*

- 1 *Cell Reports* **12**:1212–1222.
- 2 Breidenkamp N, Yang J, Clarke J, Stirparo GG, von Meyenn F, Dietmann S, Baker D, Drummond R,
3 Ren Y, Li D, Wu C, Rostovskaya M, Eminli-Meissner S, Smith A, Guo G. 2019b. Wnt
4 Inhibition Facilitates RNA-Mediated Reprogramming of Human Somatic Cells to Naive
5 Pluripotency. *Stem Cell Reports* **13**:1083–1098.
- 6 Brennan J, Lu CC, Norris DP, Rodriguez TA, Beddington RS, Robertson EJ. 2001. Nodal signalling
7 in the epiblast patterns the early mouse embryo. *Nature* **411**:965–969.
- 8 Brons IGM, Smithers LE, Trotter MWB, Rugg-Gunn P, Sun B, Chuva de Sousa Lopes SM, Howlett
9 SK, Clarkson A, Ahrlund-Richter L, Pedersen RA, Vallier L. 2007. Derivation of pluripotent
10 epiblast stem cells from mammalian embryos. *Nature* **448**:191–195.
- 11 Brown S, Teo A, Pauklin S, Hannan N, Cho CH-H, Lim B, Vardy L, Dunn NR, Trotter M, Pedersen
12 R, Vallier L. 2011. Activin/Nodal signaling controls divergent transcriptional networks in human
13 embryonic stem cells and in endoderm progenitors. *Stem Cells* **29**:1176–1185.
- 14 Cambuli F, Murray A, Dean W, Dudzinska D, Krueger F, Andrews S, Senner CE, Cook SJ,
15 Hemberger M. 2014. Epigenetic memory of the first cell fate decision prevents complete ES cell
16 reprogramming into trophoblast. *Nat Commun* **5**:5538.
- 17 Camus A, Perea-Gomez A, Moreau A, Collignon J. 2006. Absence of Nodal signaling promotes
18 precocious neural differentiation in the mouse embryo. *Dev Biol* **295**:743–755.
- 19 Castel G, Meistermann D, Bretin B, Firmin J, Blin J, Loubersac S, Bruneau A, Chevolleau S, Kilens
20 S, Chariou C, Gaignerie A, Francheteau Q, Kagawa H, Charpentier E, Flippe L, François-
21 Champion V, Haider S, Dietrich B, Knöfler M, Arima T, Bourdon J, Rivron N, Masson D,
22 Fournier T, Okae H, Fréour T, David L. 2020. Induction of Human Trophoblast Stem Cells from
23 Somatic Cells and Pluripotent Stem Cells. *Cell Rep* **33**:108419.
- 24 Chan Y-S, Göke J, Ng J-H, Lu X, Gonzales KAU, Tan C-P, Tng W-Q, Hong Z-Z, Lim Y-S, Ng H-H.
25 2013. Induction of a human pluripotent state with distinct regulatory circuitry that resembles
26 preimplantation epiblast. *Cell Stem Cell* **13**:663–675.
- 27 Chovanec P, Collier AJ, Krueger C, Várnai C, Semprich CI, Schoenfelder S, Corcoran AE, Rugg-
28 Gunn PJ. 2021. Widespread reorganisation of pluripotent factor binding and gene regulatory
29 interactions between human pluripotent states. *Nat Commun* **12**:2098.
- 30 Cinkornpumin JK, Kwon SY, Guo Y, Hossain I, Sirois J, Russett CS, Tseng H-W, Okae H, Arima T,
31 Duchaine TF, Liu W, Pastor WA. 2020. Naive Human Embryonic Stem Cells Can Give Rise to
32 Cells with a Trophoblast-like Transcriptome and Methylome. *Stem Cell Reports* **15**:198–213.
- 33 Collier AJ, Panula SP, Schell JP, Chovanec P, Plaza Reyes A, Petropoulos S, Corcoran AE, Walker
34 R, Douagi I, Lanner F, Rugg-Gunn PJ. 2017. Comprehensive Cell Surface Protein Profiling
35 Identifies Specific Markers of Human Naive and Primed Pluripotent States. *Cell Stem Cell*
36 **20**:874–890.
- 37 D'Amour KA, Agulnick AD, Eliazar S, Kelly OG, Kroon E, Baetge EE. 2005. Efficient

- 1 differentiation of human embryonic stem cells to definitive endoderm. *Nat Biotechnol* **23**:1534–
2 1541.
- 3 Davidson KC, Mason EA, Pera MF. 2015. The pluripotent state in mouse and human. *Development*
4 **142**:3090–3099.
- 5 Dawlaty MM, Ganz K, Powell BE, Hu Y-C, Markoulaki S, Cheng AW, Gao Q, Kim J, Choi S-W,
6 Page DC, Jaenisch R. 2011. Tet1 is dispensable for maintaining pluripotency and its loss is
7 compatible with embryonic and postnatal development. *Cell Stem Cell* **9**:166–175.
- 8 Di Stefano B, Ueda M, Sabri S, Brumbaugh J, Huebner AJ, Sahakyan A, Clement K, Clowers KJ,
9 Erickson AR, Shioda K, Gygi SP, Gu H, Shioda T, Meissner A, Takashima Y, Plath K,
10 Hochedlinger K. 2018. Reduced MEK inhibition preserves genomic stability in naive human
11 embryonic stem cells. *Nat Methods* **15**:732–740.
- 12 Dong C, Beltcheva M, Gontarz P, Zhang B, Popli P, Fischer LA, Khan SA, Park K-M, Yoon E-J,
13 Xing X, Kommagani R, Wang T, Solnica-Krezel L, Theunissen TW. 2020. Derivation of
14 trophoblast stem cells from naïve human pluripotent stem cells. *Elife* **9**. doi:10.7554/eLife.52504
- 15 Dong C, Fischer LA, Theunissen TW. 2019. Recent insights into the naïve state of human
16 pluripotency and its applications. *Exp Cell Res* **385**:111645.
- 17 Gafni O, Weinberger L, Mansour AA, Manor YS, Chomsky E, Ben-Yosef D, Kalma Y, Viukov S,
18 Maza I, Zviran A, Rais Y, Shipony Z, Mukamel Z, Krupalnik V, Zerbib M, Geula S, Caspi I,
19 Schneir D, Shwartz T, Gilad S, Amann-Zalcenstein D, Benjamin S, Amit I, Tanay A, Massarwa
20 R, Novershtern N, Hanna JH. 2013. Derivation of novel human ground state naive pluripotent
21 stem cells. *Nature* **504**:282–286.
- 22 Gifford CA, Ziller MJ, Gu H, Trapnell C, Donaghey J, Tsankov A, Shalek AK, Kelley DR, Shishkin
23 AA, Issner R, Zhang X, Coyne M, Fostel JL, Holmes L, Meldrim J, Guttman M, Epstein C, Park
24 H, Kohlbacher O, Rinn J, Gnirke A, Lander ES, Bernstein BE, Meissner A. 2013.
25 Transcriptional and epigenetic dynamics during specification of human embryonic stem cells.
26 *Cell* **153**:1149–1163.
- 27 Guo G, Stirparo GG, Strawbridge SE, Spindlow D, Yang J, Clarke J, Dattani A, Yanagida A, Li MA,
28 Myers S, Özel BN, Nichols J, Smith A. 2021. Human naive epiblast cells possess unrestricted
29 lineage potential. *Cell Stem Cell* **28**:1040–1056.
- 30 Guo G, von Meyenn F, Rostovskaya M, Clarke J, Dietmann S, Baker D, Sahakyan A, Myers S,
31 Bertone P, Reik W, Plath K, Smith A. 2017. Epigenetic resetting of human pluripotency.
32 *Development* **144**:2748–2763.
- 33 Guo G, von Meyenn F, Santos F, Chen Y, Reik W, Bertone P, Smith A, Nichols J. 2016. Naive
34 Pluripotent Stem Cells Derived Directly from Isolated Cells of the Human Inner Cell Mass. *Stem*
35 *Cell Reports* **6**:437–446.
- 36 Heintzman ND, Hon GC, Hawkins RD, Kheradpour P, Stark A, Harp LF, Ye Z, Lee LK, Stuart RK,
37 Ching CW, Ching KA, Antosiewicz-Bourget JE, Liu H, Zhang X, Green RD, Lobanenkov VV,

- 1 Stewart R, Thomson JA, Crawford GE, Kellis M, Ren B. 2009. Histone modifications at human
2 enhancers reflect global cell-type-specific gene expression. *Nature* **459**:108–112.
- 3 Inman GJ, Nicolás FJ, Callahan JF, Harling JD. 2002. SB-431542 is a potent and specific inhibitor of
4 transforming growth factor- β superfamily type I activin receptor-like kinase (ALK) receptors
5 ALK4, ALK5, and ALK7. *Molecular Pharmacology* **62**:65–74.
- 6 Io S, Kabata M, Iemura Y, Semi K, Morone N, Minagawa A, Wang B, Okamoto I, Nakamura T,
7 Kojima Y, Iwatani C, Tsuchiya H, Kaswandy B, Kondoh E, Kaneko S, Woltjen K, Saitou M,
8 Yamamoto T, Mandai M, Takashima Y. 2021. Capturing human trophoblast development with
9 naive pluripotent stem cells in vitro. *Cell Stem Cell* **28**:1023–1039.
- 10 James D, Levine AJ, Besser D, Hemmati-Brivanlou A. 2005. TGF β /activin/nodal signaling is
11 necessary for the maintenance of pluripotency in human embryonic stem cells. *Development*
12 **132**:1273–1282.
- 13 Ji X, Dadon DB, Powell BE, Fan ZP, Borges-Rivera D, Shachar S, Weintraub AS, Hnisz D, Pegoraro
14 G, Lee TI, Misteli T, Jaenisch R, Young RA. 2016. 3D Chromosome Regulatory Landscape of
15 Human Pluripotent Cells. *Cell Stem Cell* **18**:262–275.
- 16 Koh KP, Yabuuchi A, Rao S, Huang Y, Cunniff K, Nardone J, Laiho A, Tahiliani M, Sommer CA,
17 Mostoslavsky G, Lahesmaa R, Orkin SH, Rodig SJ, Daley GQ, Rao A. 2011. Tet1 and Tet2
18 regulate 5-hydroxymethylcytosine production and cell lineage specification in mouse embryonic
19 stem cells. *Cell Stem Cell* **8**:200–213.
- 20 Linneberg-Agerholm M, Wong YF, Romero Herrera JA, Monteiro RS, Anderson KGV, Brickman
21 JM. 2019. Naïve human pluripotent stem cells respond to Wnt, Nodal and LIF signalling to
22 produce expandable naïve extra-embryonic endoderm. *Development* **146**.
23 doi:10.1242/dev.180620
- 24 Liu X, Ouyang JF, Rossello FJ, Tan JP, Davidson KC, Valdes DS, Schröder J, Sun YBY, Chen J,
25 Knaupp AS, Sun G, Chy HS, Huang Z, Pflueger J, Firas J, Tano V, Buckberry S, Paynter JM,
26 Larcombe MR, Poppe D, Choo XY, O'Brien CM, Pastor WA, Chen D, Leichter AL, Naeem H,
27 Tripathi P, Das PP, Grubman A, Powell DR, Laslett AL, David L, Nilsson SK, Clark AT, Lister
28 R, Nefzger CM, Martelotto LG, Rackham OJL, Polo JM. 2020. Reprogramming roadmap reveals
29 route to human induced trophoblast stem cells. *Nature* **586**:101–107.
- 30 Mahadevan S, Wen S, Wan Y-W, Peng H-H, Otta S, Liu Z, Iacovino M, Mahen EM, Kyba M,
31 Sadikovic B, Van den Veyver IB. 2014. NLRP7 affects trophoblast lineage differentiation, binds
32 to overexpressed YY1 and alters CpG methylation. *Hum Mol Genet* **23**:706–716.
- 33 Mathieu J, Ruohola-Baker H. 2017. Metabolic remodeling during the loss and acquisition of
34 pluripotency. *Development* **144**:541–551.
- 35 Mesnard D, Guzman-Ayala M, Constam DB. 2006. Nodal specifies embryonic visceral endoderm and
36 sustains pluripotent cells in the epiblast before overt axial patterning. *Development* **133**:2497–
37 2505.

- 1 Niakan KK, Eggan K. 2013. Analysis of human embryos from zygote to blastocyst reveals distinct
2 gene expression patterns relative to the mouse. *Dev Biol* **375**:54–64.
- 3 Okae H, Toh H, Sato T, Hiura H, Takahashi S, Shirane K, Kabayama Y, Suyama M, Sasaki H, Arima
4 T. 2018. Derivation of Human Trophoblast Stem Cells. *Cell Stem Cell* **22**:50–63.
- 5 Pastor WA, Chen D, Liu W, Kim R, Sahakyan A, Lukianchikov A, Plath K, Jacobsen SE, Clark AT.
6 2016. Naive Human Pluripotent Cells Feature a Methylation Landscape Devoid of Blastocyst or
7 Germline Memory. *Cell Stem Cell* **18**:323–329.
- 8 Pastor WA, Liu W, Chen D, Ho J, Kim R, Hunt TJ, Lukianchikov A, Liu X, Polo JM, Jacobsen SE,
9 Clark AT. 2018. TFAP2C regulates transcription in human naive pluripotency by opening
10 enhancers. *Nat Cell Biol* **20**:553–564.
- 11 Petropoulos S, Edsgård D, Reinius B, Deng Q, Panula SP, Codeluppi S, Reyes AP, Linnarsson S,
12 Sandberg R, Lanner F. 2016. Single-Cell RNA-Seq Reveals Lineage and X Chromosome
13 Dynamics in Human Preimplantation Embryos. *Cell* **165**:1012–1026.
- 14 Ralston A, Cox BJ, Nishioka N, Sasaki H, Chea E, Rugg-Gunn P, Guo G, Robson P, Draper JS,
15 Rossant J. 2010. Gata3 regulates trophoblast development downstream of Tead4 and in parallel
16 to Cdx2. *Development* **137**:395–403.
- 17 Rossant J, Tam PPL. 2017. New Insights into Early Human Development: Lessons for Stem Cell
18 Derivation and Differentiation. *Cell Stem Cell* **20**:18–28.
- 19 Rostovskaya M, Stirparo GG, Smith A. 2019. Capacitation of human naïve pluripotent stem cells for
20 multi-lineage differentiation. *Development* **146**. doi:10.1242/dev.172916
- 21 Sahakyan A, Kim R, Chronis C, Sabri S, Bonora G, Theunissen TW, Kuoy E, Langerman J, Clark
22 AT, Jaenisch R, Plath K. 2017. Human Naive Pluripotent Stem Cells Model X Chromosome
23 Dampening and X Inactivation. *Cell Stem Cell* **20**:87–101.
- 24 Smith JR, Vallier L, Lupo G, Alexander M, Harris WA, Pedersen RA. 2008. Inhibition of
25 Activin/Nodal signaling promotes specification of human embryonic stem cells into
26 neuroectoderm. *Dev Biol* **313**:107–117.
- 27 Soncin F, Khater M, To C, Pizzo D, Farah O, Wakeland A, Arul Nambi Rajan K, Nelson KK, Chang
28 C-W, Moretto-Zita M, Natale DR, Laurent LC, Parast MM. 2018. Comparative analysis of
29 mouse and human placentae across gestation reveals species-specific regulators of placental
30 development. *Development* **145**. doi:10.1242/dev.156273
- 31 Taei A, Rasooli P, Braun T, Hassani S-N, Baharvand H. 2020. Signal regulators of human naïve
32 pluripotency. *Exp Cell Res* **389**:111924.
- 33 Takashima Y, Guo G, Loos R, Nichols J, Ficiz G, Krueger F, Oxley D, Santos F, Clarke J, Mansfield
34 W, Reik W, Bertone P, Smith A. 2014. Resetting transcription factor control circuitry toward
35 ground-state pluripotency in human. *Cell* **158**:1254–1269.
- 36 Theunissen TW, Friedli M, He Y, Planet E, O’Neil RC, Markoulaki S, Pontis J, Wang H, Iouranova
37 A, Imbeault M, Duc J, Cohen MA, Wert KJ, Castanon R, Zhang Z, Huang Y, Nery JR, Drotar J,

- 1 Lungjangwa T, Trono D, Ecker JR, Jaenisch R. 2016. Molecular Criteria for Defining the Naive
2 Human Pluripotent State. *Cell Stem Cell* **19**:502–515.
- 3 Theunissen TW, Powell BE, Wang H, Mitalipova M, Faddah DA, Reddy J, Fan ZP, Maetzel D, Ganz
4 K, Shi L, Lungjangwa T, Imsoonthornruksa S, Stelzer Y, Rangarajan S, D'Alessio A, Zhang J,
5 Gao Q, Dawlaty MM, Young RA, Gray NS, Jaenisch R. 2014. Systematic Identification of
6 Culture Conditions for Induction and Maintenance of Naive Human Pluripotency. *Cell Stem Cell*
7 **15**:524–526.
- 8 Thomson JA, Itskovitz-Eldor J, Shapiro SS, Waknitz MA, Swiergiel JJ, Marshall VS, Jones JM. 1998.
9 Embryonic stem cell lines derived from human blastocysts. *Science* **282**:1145–1147.
- 10 Touboul T, Hannan NRF, Corbineau S, Martinez A, Martinet C, Branchereau S, Mainot S, Strick-
11 Marchand H, Pedersen R, Di Santo J, Weber A, Vallier L. 2010. Generation of functional
12 hepatocytes from human embryonic stem cells under chemically defined conditions that
13 recapitulate liver development. *Hepatology*. doi:10.1002/hep.23506
- 14 Vallier L, Alexander M, Pedersen RA. 2005. Activin/Nodal and FGF pathways cooperate to maintain
15 pluripotency of human embryonic stem cells. *J Cell Sci* **118**:4495–4509.
- 16 Vallier L, Mendjan S, Brown S, Chng Z, Teo A, Smithers LE, Trotter MWB, Cho CH-H, Martinez A,
17 Rugg-Gunn P, Brons G, Pedersen RA. 2009. Activin/Nodal signalling maintains pluripotency by
18 controlling Nanog expression. *Development* **136**:1339–1349.
- 19 Vallot C, Patrat C, Collier AJ, Huret C, Casanova M, Liyakat Ali TM, Tosolini M, Frydman N, Heard
20 E, Rugg-Gunn PJ, Rougeulle C. 2017. XACT Noncoding RNA Competes with XIST in the
21 Control of X Chromosome Activity during Human Early Development. *Cell Stem Cell* **20**:102–
22 111.
- 23 Varlet I, Collignon J, Robertson EJ. 1997. nodal expression in the primitive endoderm is required for
24 specification of the anterior axis during mouse gastrulation. *Development* **124**:1033–1044.
- 25 Weinberger L, Ayyash M, Novershtern N, Hanna JH. 2016. Dynamic stem cell states: naive to primed
26 pluripotency in rodents and humans. *Nat Rev Mol Cell Biol* **17**:155–169.
- 27 Wojdyla K, Collier AJ, Fabian C, Nisi PS, Biggins L, Oxley D, Rugg-Gunn PJ. 2020. Cell-Surface
28 Proteomics Identifies Differences in Signaling and Adhesion Protein Expression between Naive
29 and Primed Human Pluripotent Stem Cells. *Stem Cell Reports* **14**:972–988.
- 30 Xiang L, Yin Y, Zheng Y, Ma Y, Li Y, Zhao Z, Guo J, Ai Z, Niu Y, Duan K, He J, Ren S, Wu D, Bai
31 Y, Shang Z, Dai X, Ji W, Li T. 2020. A developmental landscape of 3D-cultured human pre-
32 gastrulation embryos. *Nature* **577**:537–542.
- 33 Xu R-H, Sampsel-Barron TL, Gu F, Root S, Peck RM, Pan G, Yu J, Antosiewicz-Bourget J, Tian S,
34 Stewart R, Thomson JA. 2008. NANOG Is a Direct Target of TGF β /Activin-Mediated SMAD
35 Signaling in Human ESCs. *Cell Stem Cell* **3**:196–206.
- 36 Zhao C, Reyes AP, Schell JP, Weltner J, Ortega N. 2021. Reprogrammed iBlastoids contain amnion-
37 like cells but not trophectoderm. *bioRxiv*. doi:10.1101/2021.05.07.442980